Implementing belowground controls on nutrient uptake in a land surface model improves representation of a boreal peatland ecosystem

Yaoping Wang¹, Daniel M. Ricciuto¹, Jiafu Mao¹, Sören E. Weber², Verity G. Salmon¹, Xiaoying Shi¹, Xiaojuan Yang¹, Natalie A. Griffiths¹, Paul J. Hanson¹, Katherine Duchesneau³, Camille E. Defrenne⁴, Jeffrey M. Warren¹, Stephen D. Sebestyen⁵, Keith Oleheiser¹, Melanie A. Mayes¹, Peter Thornton¹

Correspondence to: Yaoping Wang (wangy7@ornl.gov), Jiafu Mao (maoj@ornl.gov)

Copyright notice: This manuscript has been authored by UT-Battelle, LLC, under Contract No. DE-AC05-00OR22725 with the U.S. Department of Energy. The US Government retains and the publisher, by accepting the article for publication, acknowledges that the US Government retains a non-exclusive, paid-up, irrevocable, worldwide license to publish or reproduce the published form of this manuscript, or allow others to do so, for US Government purposes. The Department of Energy will provide public access to these results of federally sponsored research in accordance with the DOE Public Access Plan (http://energy.gov/downloads/doe-public-access-plan, last access: 2025/11/14).

¹Environmental Sciences Division, Oak Ridge National Laboratory, Oak Ridge, TN, 37830, USA

²Department of Biology, West Virginia University, Morgantown, WV, 26505, USA

³School of Integrative Plant Science, Cornell University, NY, 14850, USA

⁴RECON environmental, Inc., San Diego, CA, 92108, USA

⁵ Northern Research Station, U.S. Department of Agriculture Forest Service, Grand Rapids, MN, 55744, USA

1	Supple	ementary Text	3
	1.1 Nu	trient uptake modifications	3
	1.1.1	Preliminary notes	3
	1.1.2	Nutrient uptake and plant C balance in ELM-OLD	3
	1.1.3	Nutrient limitation of the soil-decomposition process in ELM-OLD and ELM-MYCI	6
	1.1.4	Overview of the nutrient uptake and plant C balance in ELM-MYCI	6
	1.1.5	Colonization rates by ectomycorrhizal and ericoid fungi	7
	1.1.6	Common environmental multipliers	8
	1.1.7	Acquisition of nutrient from soil inorganic and organic sources via mycorrhizal roots	9
	1.1.8	Upper bound on the nonstructural carbohydrate cost of N acquisition via mycorrhizal roots	12
	1.1.9	Reduction of soil organic N content due to the acquisition of mycorrhizal roots	13
	1.1.10	Direct uptake of inorganic nutrients by uncolonized fine roots	13
	1.2 Re	moval of pretreatment variability	14
2	Supple	ementary Tables	14
3	Supple	ementary Figures	22
4	Refere	nces	31

1 Supplementary Text

1.1 Nutrient uptake modifications

1.1.1 Preliminary notes

The same processes apply to nitrogen (N) and phosphorus (P). The description below (Sect. 1.1.2 to 1.1.10) focuses on N. The description for P can be obtained by substituting out all N by P in the text and equations, except when specifically pointed out. The capitalized letters in all the equations are modelled variables and will be explained as they appear. The meanings of subscripts are consistent throughout and are as follows:

i – soil layer

j – plant functional type (PFT), $j \in \{\text{spruce, tamarack, shrub, moss}\}$, or, when describing the new equations in ELM-MYCI, $j \in \{\text{spruce, tamarack, shrub}\}$, since moss is not modified

m – means the term is for soil decomposition

h - plant litter pool, $h \in \{lab, cel, lig\}$, lab - labile, cel - cellulose, lig - lignin

The model time step is $\Delta t = 3600$ seconds (1 hour). The lower-case letters that are not Δt or in the subscript are model parameters and will be explained as they appear. Parameter values are summarized in Table S2-Table S5.

1.1.2 Nutrient uptake and plant C balance in ELM-OLD

Black + blue colours in Figure S1 show the calculations used to determine nutrient uptake in the default ELMv2-SPRUCE (ELM-OLD). Net photosynthesis is divided by the whole plant's C:N ratio to calculate the corresponding necessary N to support structural growth in leaf, stem, coarse root, and fine root C (Burrows et al., 2020). This growth demand for N is first met by retranslocation, and the remaining part becomes plant's demand for inorganic N, see Eq. (S1). Within a soil column, all the plant functional types (PFTs) and the soil decomposition processes compete for the same pool of soil inorganic N following the "Relative Demand" scheme (Burrows et al., 2020; Thornton and Rosenbloom, 2005). That is, the model first calculates a total potential N uptake by all the PFTs and soil decomposition (Eq. (S2)-(S3); also see Sect. 1.1.3). If the total potential N uptake is greater than the available soil inorganic N, the individual potential uptakes are all scaled down by the same column-level limitation factor, F_{Nlimit} , to obtain the actual uptakes, $N_{upt,act,j}$ (Eq. (S4)-(S6)). Under soil inorganic N or P limitation, plant structural growth is constrained to the lower of the two growth levels permitted by total N and P availability, i.e., the total of retranslocation and actual NP uptake, see Eq. (S7).

The calculation of each PFT's C balance is interwoven with the nutrient uptake calculations (Figure S2). At the centre is the nonstructural carbohydrates (NSC) pool, which receives new C from gross primary productivity (GPP), and supplies C to maintenance respiration (MR), excess respiration (XR), growth respiration (GR), structural C growth, and recovery of a virtual "XSMR" pool. MR reflects the metabolic energy spent to maintain a plant's regular functions, and increases approximately linearly with total living biomass. XR reflects the wasted energy due to nutrient limitation and increases exponentially up to a constant with the percentage of plant biomass existing as NSC. Both MR and XR also increase exponentially with temperature. GR reflects the energy spent to synthesize new biomaterials for structural growth and is a small and constant fraction of structural growth. The "XSMR" pool is a virtual pool,

defined for numerical purposes, to prevent the NSC pool from going negative when MR exceeds GPP for prolonged periods (e.g., in winter). Whenever MR > GPP, the unmet MR demand is subtracted from the XSMR pool instead of the NSC pool. This often causes the XSMR pool to go negative. To replenish the XSMR pool, when GPP > MR, some C is taken out of the NSC pool to slowly replenish it according to fixed rules. In this way, the XSMR pool has a small impact on net primary productivity (NPP), but it is not a physical pool or part of the plants' biomass.

$$N_{demand,inorg,j} = \max \left(\frac{C_{net}}{CN_i} - N_{retrans,j}, 0 \right) \quad \forall j$$
 (S1)

$$N_{upt,pot,j} = N_{demand,inorg,j} \quad \forall j$$
 (S2)

$$N_{upt,pot} = N_{upt,pot,m} + \sum_{j} N_{upt,pot,j}$$
 (S3)

$$F_{Nlimit} = \min(N_{soil}/(N_{upt,pot} \cdot \Delta t), 1)$$
 (S4)

$$N_{upt,act,j} = F_{Nlimit} N_{upt,pot,j} \quad \forall j$$
 (S5)

$$N_{upt.act.m} = F_{Nlimit} N_{upt.pot.m}$$
 (S6)

 $\Delta C_{structural,j}$

$$= \begin{cases} C_{net} \cdot \Delta t & \text{if } \min(F_{Nlimit}, F_{Plimit}) = 1 \\ \min\left(\frac{CN_j \cdot \Delta t}{N_{upt,act,j} + N_{retrans,j}}, \frac{CP_j \cdot \Delta t}{P_{upt,act,j} + P_{retrans,j}}\right) & \text{if } \min(F_{Nlimit}, F_{Plimit}) < 1 \end{cases}$$
(S7)

 $C_{net,j}$ – incoming net photosynthesis, g C m⁻² s⁻¹

 CN_i – the whole plant's C:N ratio, unitless

N_{retrans,j} - N supply from retranslocation, g N m⁻² s⁻¹

 $N_{demand,inorg,j}$ – plant demand for inorganic N, g N m⁻² s⁻¹

N_{upt.pot.i} – potential plant inorganic N uptake, g N m⁻² s⁻¹

 $N_{uvt.vot.m}$ – potential soil decomposition inorganic N uptake, g N m⁻² s⁻¹

 $N_{upt,pot}$ – total potential plant and soil decomposition inorganic N uptake, g N m⁻² s⁻¹

 N_{soil} – size of the column-level inorganic N pool (the sum of NH₄⁺, NO₃⁻, and biological N fixation; for P, this is soluble P [PO₄³⁻]), g N m⁻²

 F_{Nlimit} – column-level N-limitation factor, unitless

 $N_{upt,act,j}$ – actual plant inorganic N uptake, g N m⁻² s⁻¹

 $N_{upt,act,m}$ – actual soil decomposition inorganic N uptake, g N m⁻² s⁻¹

 $\Delta C_{structural,j}$ – structural growth of the plant in the time step, g C m⁻²

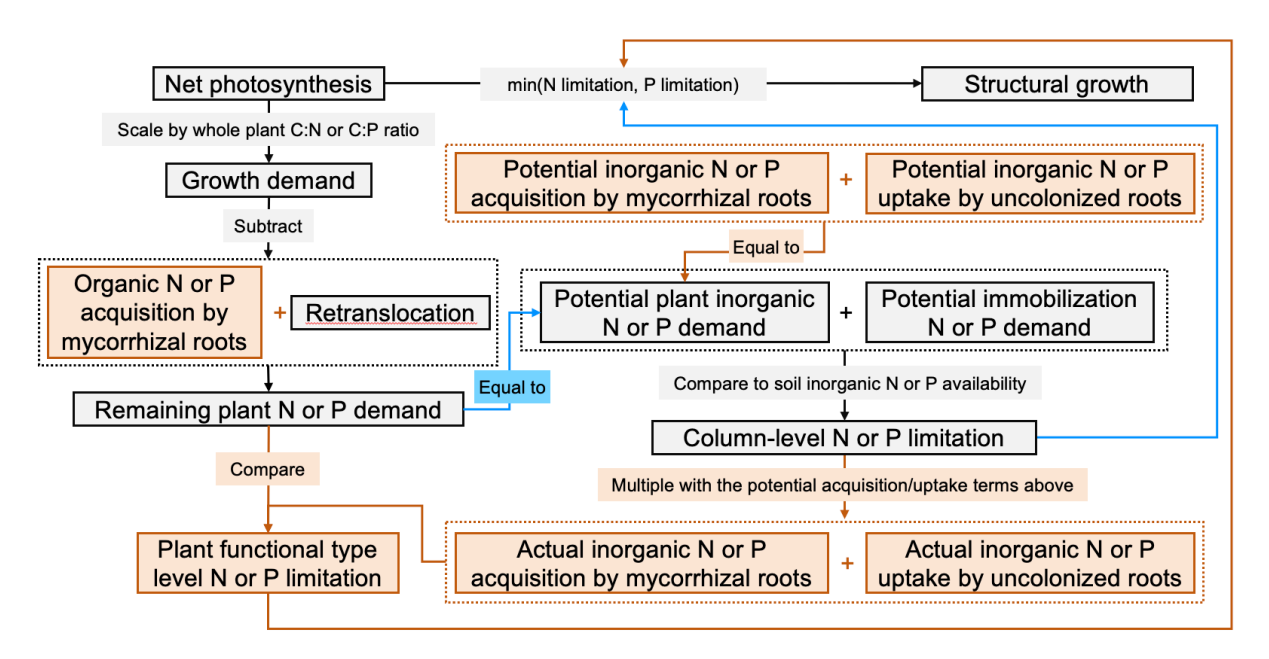


Figure S1. Nutrient uptake processes by the vascular plant functional types in ELM-OLD and ELM-MYCI. Boxes with edge are modelled quantities, lines and boxes without edge are calculations. Black boxes and lines are shared processes, blue ones exist only in ELM-OLD, and orange ones exist only in ELM-MYCI.

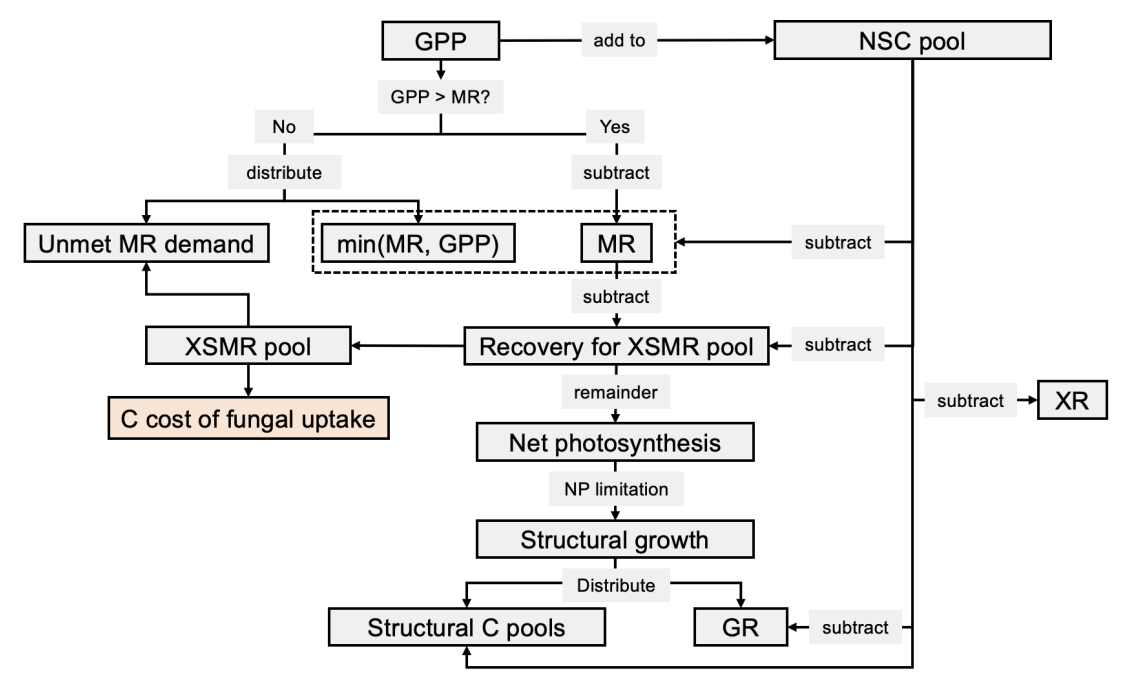


Figure S2. Relationship between the terms involved in the N and P uptake calculations (net photosynthesis and structural growth) and the terms involved in C-balance calculations (the other terms in this figure). Black boxes are terms shared by ELM-OLD and ELM-MYCI. The orange box is a new flux out of the XSMR pool in ELM-MYCI. Abbreviations: $GPP-gross\ primary\ productivity,\ MR-maintenance\ respiration,\ XR-excess\ respiration,\ GR-growth\ respiration,\ NSC-nonstructural\ carbohydrates.$

1.1.3 Nutrient limitation of the soil-decomposition process in ELM-OLD and ELM-MYCI

Although soil decomposition processes are not modified in this study, and the full scheme is described elsewhere (Burrows et al., 2020; Oleson et al., 2013), a brief overview is provided here to contextualize heterotrophic respiration (HR) and its dependence on nutrient availability. ELMv2-SPRUCE uses the Converging Trophic Cascade scheme, which has one coarse woody debris pool, three plant litter pools (conceptualized as labile, cellulose, and lignin), and four soil organic matter (SOM) pools (Burrows et al., 2020; Oleson et al., 2013). C flows from upstream to downstream pools, in the approximate order of woody debris → plant litter → faster-turnover SOM → slower-turnover SOM, following first-order exponential decay. The C:N and C:P ratios of the coarse woody debris and plant litter pools are flexible and determined by the input plant materials. The C:N and C:P ratios of the SOM pools are fixed parameters (Table S2).

During each transformation, a fraction of the upstream carbon is released as CO_2 , in proportion to the pool size and the transformation rate. HR is calculated as the sum of these CO_2 fluxes across all transformations and soil layers. Each transformation also generates N and P demands ($N_{upt,pot,m}$ in Eq. (S3), immobilization demand in Figure S1), because the upstream pools generally have higher C:N and C:P ratios than the downstream pools. To satisfy these stoichiometric requirements, additional N and P must be obtained from the soil inorganic pool. Nutrient limitation of the transformation rate, and thus HR, occurs when the available soil inorganic N or P is insufficient to meet the combined demands of plants and decomposition (Eq. (S4)).

1.1.4 Overview of the nutrient uptake and plant C balance in ELM-MYCI

In the modified ELMv2-SPRUCE (ELM-MYCI), we split the nutrient uptake processes of the vascular PFTs (spruce, tamarack, and shrubs) into three pathways: (1) direct inorganic nutrient uptake by uncolonized fine roots (PATH^{root}), (2) indirect inorganic nutrient acquisition by mycorrhizal roots (PATH^{myc,inorg}), and (3) indirect nutrient acquisition from organic sources by mycorrhizal roots (PATH^{myc,org}). This split is based on the idea that EcM fungal mantle can prevent fine roots from accessing the soil solution (He et al., 2018). The uncolonized fine roots can only use PATH^{root}, whereas the fungi-colonized fine roots can only use PATH^{myc,inorg} and PATH^{myc,org}. Pathways (2) and (3) are mycorrhizal-implicit. They do not consider fungal biomass dynamics or explicit exchanges of C-N-P between the plant host and fungi. Instead, they treat the fungal uptake of inorganic nutrient, or mining of organic nutrient, and subsequent transfer to the plant host via the colonized fine roots as a lumped process. The plant host pays a C cost for the fungi-mediated nutrient acquisitions from the XSMR pool (Figure S2 orange box), but this cost is not allocated to fungal biomass or soil respiration because doing so appropriately would require modifying the soil decomposition scheme (Sect. 1.1.3). Nutrient uptake and the C balance for the non-vascular *Sphagnum* moss remains the same as in ELM-OLD, Eq. (S3)-(S7).

We embed the three pathways into the broader model as shown in Figure S1 (orange boxes). We first modify Eq. (S1) to let the growth demand for N be first met by retranslocation and PATH^{myc,org}, Eq. (S8). The remainder becomes the plant's demand for inorganic N. This order of subtraction gives the plant a preference of organic N over inorganic N, which we deem acceptable for the boreal peatland ecosystem because it has abundant organic matter. Under the

current code structure of ELMv2-SPRUCE, removing this assumption will require revising both the nutrient competition and soil decomposition calculations, which is beyond the scope of this study. We then replace Eq. (S2) with Eq. (S9), where the new potential inorganic N uptake is the sum of two potential uptake terms, one via PATH^{root} and one via PATH^{myc,inorg}. After scaling down the potential inorganic N uptake by soil N availability, Eq. (S4)-(S6), we obtain the actual inorganic N uptake via PATH^{root} and PATH^{myc,inorg}. The sum of retranslocation, the actual inorganic N uptake via fine roots, the actual inorganic N acquisition via mycorrhizal roots, and the organic N acquisition via mycorrhizal roots becomes the total N supplied to the plants for structural growth, Eq. (S10). With those modifications, we obtain PFT-specific nutrient-limitation factors, Eq. (S11), as opposed to only the column level one in Eq. (S4) in ELM-OLD.

$$N_{demand,inorg,j} = \max \left(\frac{C_{net}}{CN_j} - N_{retrans,j} - N_{myc,org,j}, 0 \right) \quad \forall j$$
 (S8)

$$N_{upt,pot,j} = N_{froot,j} + N_{myc,inorg,j}$$
 (S9)

$$\Delta C_{structural,j} = \begin{cases} C_{net} \cdot \Delta t & \text{if } F_{Nlimit} = 1\\ CN_j \cdot \Delta t & \text{if } F_{Nlimit} < 1 \end{cases}$$

$$(S10)$$

$$F_{Nlimit,j} = \begin{cases} 1 & \text{if } N_{demand,inorg,j} = 0\\ \frac{N_{upt,act,j}}{N_{demand,inorg,j}} & \text{if } N_{demand,inorg,j} > 0 \end{cases}$$
(S11)

 $N_{myc,org,i}$ – N acquisition from organic sources through mycorrhizal roots, g N m⁻² s⁻¹

 $N_{myc,inorg,j}$ – potential inorganic N acquisition through mycorrhizal roots, g N m⁻² s⁻¹

 $N_{froot,j}$ – potential uptake of inorganic N through uncolonized fine roots, g N m⁻² s⁻¹

 $F_{Nlimit,j}$ – PFT-specific N limitation factor, unitless

1.1.5 Colonization rates by ectomycorrhizal and ericoid fungi

Operationalizing Eq. (S8)-(S11) requires modelling the fraction of roots that are uncolonized, i.e. using PATH^{myc,inorg} and PATH^{myc,org}. At the SPRUCE site, observations found that the total abundance of dark fungal hyphae, which could be ErM in origin and from *Cenococcum geophilum*, declined by 75-100% from the unheated to the warmest chamber (Defrenne et al., 2021). SPRUCE observations also found shrub roots to vastly increase in total and specific root length in the warmer enclosures, indicating a shift towards the do-it-yourself strategy (Malhotra et al., 2020; Weber et al., 2025). Other past experiments found peatland ericaceous shrubs to uptake less N via ErM fungi under inorganic N addition (Vesala et al., 2021). Based on these studies, we have relatively high confidence that ErM colonization of shrub roots decreases towards the warmer enclosures. Observed root-tip colonization rates for the EcM trees are very noisy and do not show clear trends across warming treatments (Figure S9). Also, past experiments found both increases and decreases in EcM colonization under N additions, possibly related to the amount of added N and water conditions (Table S1).

Based on the above information, we initially tested two ways to model fungal colonization rates: a linear function of annual average water table depth, or a linear function of annual average soil inorganic N content. The first approach turned out to be inviable because it induced little gradient across the treatment chambers. Therefore, we chose the

second approach, see Eq. (S12). We use the average soil inorganic N content over 0-30 cm because it is the rooting zone at the SPRUCE site (Iversen et al., 2018). For parameter optimization, we constrain the slope of response to be $b_j < 0$ for ErM colonization of shrubs but does not impose such constraint for the trees (Table S5). We choose not to include a soil P content control on mycorrhizal colonization in this study, because the study site's dependence on P is less well-understood and fewer prior studies have focused on P (Table S1), but we put a zero-coefficient into the code as placeholder for potential addition of P control in the future.

$$M_{myc,j} = \max(0, \min(1, a_j + b_j N_{soil,annavg}))$$
 (S12)

 $M_{mvc,i}$ – fraction of fine roots colonized by mycorrhizal fungi, unitless

 $N_{soil,annavg}$ – annual average soil inorganic N $(NH_4^+ + NO_3^-)$ content in the rooting zone, g N m⁻³

 a_i – intercept parameter

 b_i – slope parameter

Table S1. Review of previous studies on the influences of moisture and nutrients to EcM colonization of boreal trees.

Plant type	Treatment	Outcome	Study
Pinus sylvestris	N addition, 3-50 kg N ha ⁻¹ yr ⁻¹	No change in colonization	(Forsmark et al., 2021)
Forest stands including sugar maple, beech, yellow birch, black spruce, moss and ErM shrub understory	N addition, 9-85 kg N ha ⁻¹ yr ⁻¹	Small increase in abundance, possibly driven by tree growth	(Renaudin et al., 2023)
Picea mariana	N addition, 9-30 kg N ha ⁻¹ yr ⁻¹	Small increase in fraction of colonized root tips	(Rossi et al., 2012)
Picea asperata	Watering gradient (40-100% field capacity) x N addition gradient (0-400 kg N ha ⁻¹ yr ⁻¹)	Higher EcM colonization rates in drier treatments. Lower colonization rates under N addition	(Xie et al., 2021)
Pinus sylvestris	N addition at 100 kg N ha ⁻¹ yr ⁻¹	Lower EcM colonization rates	(Högberg et al., 2010)

1.1.6 Common environmental multipliers

We apply the following common environmental multipliers when modelling the uptake/acquisition of all three pathways: soil temperature, soil moisture, and the plant's N limitation in the previous time step. The former two multipliers are soil layer specific. The soil temperature multiplier is a conventional Q₁₀ function, Eq. (S13). The soil moisture multiplier, from (Frolking et al., 2002), is selected because the formula lets both dry soil and excess moisture to inhibit nutrient uptake, Eq. (S14). The inhibition of waterlogging on nutrient uptake is supported by observational evidence (Struyf et al., 2011). The third multiplier is a feedback mechanism that makes the modelled PFTs ramp up

uptake/acquisition rates in a nutrient-poor environment while preventing them from infinitely accumulating nutrients when demands are already met, Eq. (S15). It is weakly supported by experimental observations that high tissue nutrient concentrations inhibit plant nutrient uptake (Glass et al., 2002). Figure S3 shows the form of Eq. (S15) under various α -values. In the absence of suitable observational references and noting that the parameter does not have a large impact on model results in one-at-a-time sensitivity analysis (Figure S4), we chose $\alpha = 1.5$.

$$\mathcal{F}(T_{soi,i}) = q_{10}^{(T_{soi,i}-10)/10}$$
(S13)

$$\mathcal{F}(\Theta_{soi,i}) = \begin{cases} 1 - \left(\frac{\theta_{opt} - \Theta_{soi,i}}{\theta_{opt}}\right)^2 & \text{if } \Theta_{soi,i} \le \theta_{opt} \\ 1 - 0.5 \left(\frac{\Theta_{soi,i} - \theta_{opt}}{1 - \theta_{opt}}\right) & \text{if } \Theta_{soi,i} > \theta_{opt} \end{cases}$$
(S14)

$$\mathcal{F}(F_{Nlimit,j}) = \frac{\alpha}{F_{Nlimit,j}^2 + \alpha - 1}$$
 (S15)

 $T_{soi,i}$ – soil temperature of layer i, °C

 q_{10} – Q_{10} parameter for temperature sensitivity of nutrient uptake

 $\Theta_{soi,i}$ – volumetric soil water content in soil layer i, m³ m⁻³

 θ_{opt} – optimal soil volumetric water content for nutrient uptake, m³ m⁻³

 α – parameter controlling the feedback of excessive nutrient uptake on uptake rates

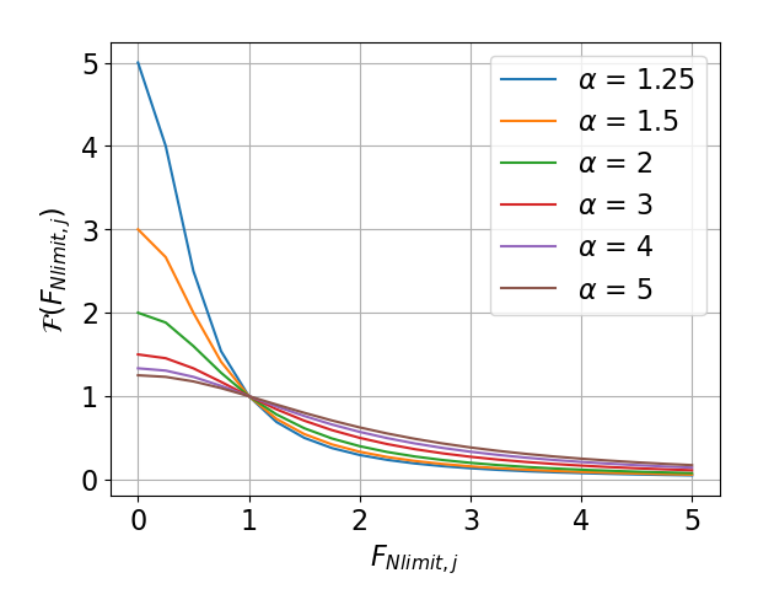


Figure S3. Visualization of the N limitation multiplier, Eq. (S15), at different parameter values.

1.1.7 Acquisition of nutrient from soil inorganic and organic sources via mycorrhizal roots

Mycorrhizal fungi growth, and hence their ability to obtain soil nutrients, depend partially on C transfer from the plants (He et al., 2018, 2021; Shao et al., 2023). In our implicit approach, we account for this phenomenon by applying a multiplier based on NSC availability (Eq. (S16)) and an upper bound based on the availability of new photosynthates (Sect. 1.1.8) on the acquisition rates of PATH^{myc,inorg} and PATH^{myc,org}. In Eq. (S16), when a PFT has high NSC

compared to its structural biomass C in leaf and fine root, the multiplier approaches one, and in the opposite situation, zero.

$$\mathcal{F}(C_{ns,j}) = \frac{k_{nsc}C_{ns,j}}{k_{nsc}C_{ns,j} + C_{froot,j} + C_{leaf,j}}$$
(S16)

 k_{nsc} – unitless sensitivity parameter

 $C_{ns,j}$ – nonstructural carbohydrates content, g C m⁻²

 $C_{froot,j}$ – displayed fine-root carbon biomass, g C m⁻²

 $C_{leaf,j}$ – displayed leaf-carbon biomass, g C m⁻²

In each soil layer, the potential N acquisition rate via PATH^{myc,org} is a function of the amount of ErM- or EcM-colonized fine-root biomass, $M_{myc,j}C_{froot,j}f_{froot,i,j}$, the environmental multipliers (Sect. 1.1.6), and the NSC multiplier, see Eq. (S17). The fraction of fine-root biomass in each soil layer, $f_{froot,i,j}$, is set using linear vertical rooting profiles, Eq. (S18), that are fitted on in situ minirhizotron data (Weber et al., 2025). The actual N acquisition rate via PATH^{myc,org} in each soil layer is limited by the sizes of soil organic N pools and the fraction of those pools that can be accessed, Eq. (S19)-(S20), using the high bound 0.0001 in the CoupModel (He et al., 2018). The total actual N acquisition rate via PATH^{myc,org} is calculated as the sum over all soil layers, Eq. (S21), followed by a final adjustment that prevents unnecessary uptake during nighttime and dormancy (see Sect. 1.1.8).

We restrict the mycorrhizal-available soil organic N pools to the three plant litter pools in the soil decomposition scheme (Sect. 1.1.3). This is because those three pools allow flexible C:N and C:P ratios, while the four SOM pools require fixed C:N and C:P ratios. To allow N and P acquisition from the SOM pools require considering how much C to release as fungal respiration. However, the current first-order decomposition processes in ELMv2-SPRUCE have no explicit microbial pools; as such, it is uncertain how much of the HR already reflects fungal respiration in the real world. There may also be difference between EcM and ErM in the fraction of released C (Clemmensen et al., 2021). Due to those difficulties, we leave the treatment of the SOM pools to future model development.

In the real world, ErM has limited ability to degrade lignin/lignin-like *Sphagnum* phenolics and other complex biopolymers (Ward et al., 2022). However, the lignin pool in ELMv2-SPRUCE is more of an abstract pool based on a decay rate than the real lignin compound (Oleson et al., 2013). Preventing the ErM-shrub association from accessing this pool will make its accessibility to organic N and P unrealistically low. Therefore, we allow the EcM-tree and ErM-shrub association to access all the litter pools.

$$N_{myc,pot,org,i,j} = u_{N,myc,j} M_{myc,j} C_{froot,j} F_{froot,i,j} \mathcal{F}(T_{soi,i}) \mathcal{F}(\Theta_{soi,i}) \mathcal{F}(F_{Nlimit,j}) F(C_{ns,j})$$
 (S17)

$$F_{froot,i,j} = \begin{cases} a_{root}(z_i - z_{i-1}) & \text{if } i > 1 \text{ or } b_{root} < 0\\ a_{root}z_i + b_{root} & \text{if } i = 1 \text{ and } b_{root} > 0 \end{cases}$$
(S18)

$$N_{avail,org,i,j} = \frac{0.0001}{\Delta t} \left(O_{N,i,lab} + O_{N,i,cel} + O_{N,i,lig} \right)$$
 (S19)

$$N_{pre,myc,org,i,j} = \min(N_{myc,pot,org,i,j}, N_{avail,org,i,j})$$
 (S20)

$$N_{pre,myc,org,j} = \sum_{i=1}^{10} N_{pre,myc,org,i,j}$$
 (S21)

 $N_{myc,pot,org,i,j}$ – potential N acquisition from organic sources via mycorrhizal roots in one soil layer, g N m⁻²

 $u_{N,myc,j}$ – the maximum organic N acquisition rate per unit colonized fine-root biomass, gN g C⁻¹ s⁻¹

 $F_{froot,i,j}$ – fraction of fine root in one soil layer, unitless

 a_{root} – slope parameter of cumulative fine-root distribution

 b_{root} – intercept parameter of cumulative fine-root distribution

 z_i – the bottom depth of the soil layer, m

 $N_{avail,org,i,j}$ – soil organic N pool size available to the plant-fungi association, g N m⁻²

 $O_{N,i,lab}$ – soil organic N pool size in the labile litter pool in the soil layer, g N m⁻²

 $O_{N,i,cel}$ – soil organic N pool size in the cellulose litter pool in the soil layer, g N m⁻²

 $O_{N,i,lig}$ – soil organic N pool size in the lignin litter pool in the soil layer, g N m⁻²

 $N_{pre,myc,org,i,j}$ – the pre-adjustment actual acquired N from organic sources via mycorrhizal roots in one soil layer, g N m⁻²

 $N_{pre,myc,org,j}$ – the pre-adjustment actual acquired N from organic sources via mycorrhizal roots over all the soil layers, gN m⁻²

Because inorganic N is much more scarce than organic N in peatland ecosystems, we limit the potential N acquisition rate by PATH^{myc,inorg} by a Michaelis-Menten multiplier, Eq. (S22). The other terms in the calculation, Eq. (S23), are the same as those in the calculation of potential organic N acquisition rate, Eq. (S17). The potential acquisition rates are summed up over all the soil layers, Eq. (S24), and subject to a final adjustment (see Sect. 1.1.8).

Constraining the rate constant $(v_{N,fungi,j})$ and half-saturation point $(k_{N,j})$ in the Michaelis-Menten multiplier is difficult. Experimentally observed rate constants vary by three orders of magnitude $(10^{-12} \text{ to } 10^{-9} \text{ g N cm}^{-2} \text{ s}^{-1} \text{ and } 10^{-13} \text{ to } 10^{-10} \text{ g P cm}^{-2} \text{ s}^{-1})$, and half-saturation points vary by one order of magnitude $(0.25\text{-}3.338 \text{ g N m}^{-3} \text{ water}, 0.049\text{-}0.17 \text{ g P m}^{-3} \text{ water})$ (Table S6-Table S7). Therefore, we first use hand-tuning to determine approximate guesses for those parameters. Then, during parameter optimization, we set the upper and lower bounds to be [0.1, 10] of the initial guesses of the rate constants, and [0.5, 2] of the initial guesses of the half-saturation points (Table S4-Table S5).

We do not distinguish between NH₄⁺ and NO₃⁻ when calculating the N acquisition rate by PATH^{myc,inorg}. The concentration of NO₃⁻ is near-zero compared to NH₄⁺ in the SPRUCE ecosystem (main text Figure 2), and plants exhibit plasticity and acclimation in their N-form preference (Chalk and Smith, 2021; Daryanto et al., 2019). As such, we deem differentiating between these two chemical forms to be an unnecessary complexity.

$$\mathcal{F}_{j}(N_{conc,i}) = \frac{N_{conc,i}}{k_{N,j} + N_{conc,i}}$$
 (S22)

$$N_{myc,pot,inorg,i,j} = v_{N,myc,j} M_{myc,j} C_{froot,j} F_{froot,i,j} \mathcal{F}_j (N_{conc,i}) \mathcal{F}(T_{soi,i}) \mathcal{F}(\Theta_{soi,i}) \mathcal{F}(F_{Nlimit,j}) F(C_{ns,j})$$
(S23)

$$N_{pre,myc,inorg,j} = \sum_{i=1}^{10} N_{myc,pot,inorg,i,j}$$
 (S24)

 $N_{conc,j}$ – soil inorganic N concentration ($NH_4^+ + NO_3^-$; for P, PO_4^{3-}) in one soil layer, g N m⁻³

 $k_{N,j}$ – half-saturation point for inorganic N uptake/acquisition, including via mycorrhizal roots and uncolonized fine roots, g N m⁻³

 $N_{myc,pot,inorg,i,j}$ – potential inorganic N acquisition via mycorrhizal roots in one soil layer, g N m⁻² s⁻¹

 $v_{N,myc,j}$ – maximum inorganic N acquisition rate per unit colonized fine-root biomass, g N g C⁻¹ s⁻¹

 $N_{pre,myc,inorg,j}$ – pre-adjustment inorganic N acquisition via mycorrhizal roots over all the soil layers, g N m⁻² s⁻¹

1.1.8 Upper bound on the nonstructural carbohydrate cost of N acquisition via mycorrhizal roots

In addition to letting the plant's NSC abundance influence the acquisition rates of PATH^{myc,inorg} and PATH^{myc,org}, Eq. (S16), we impose an upper bound on the total N acquisition from inorganic and organic sources via mycorrhizal associations due to their C cost to the plants. That is, the total acquired N from organic and inorganic sources, multiplied by a constant factor, c_N , must not exceed 50% of the net photosynthesis at each time step (C_{net} , defined in the beginning of Sect. 1.1.2), see Eq. (S25)-(S29). We choose the 50% threshold following the maximum value found in a previous meta-analysis (Hawkins et al., 2023). The use of net photosynthesis in the upper bound prevents nutrient acquisition during the night and during winter dormancy. The scaled-down inorganic N acquisition, combined with direct fine-root N uptake, undergo competition with soil decomposition, which is already described in Eq. (S9) and (S5). The total C cost to the plant is equal to the greater value between the total C cost of N acquisitions and the total C cost of P acquisitions via PATH^{myc,inorg} and PATH^{myc,org}, Eq. (S30).

We subtract the C cost from the virtual XSMR pool (see Sect. 1.1.2) in this study, which has a damped negative effect on the NSC pool – if all other model terms are held constant, a more negative XSMR pool will incur more frequent replenishments from the NSC pool to the XSMR pool (Figure S2). We do not subtract from the NSC pool directly, because negative NSC pool sizes will cause numerical problems in ELMv2-SPRUCE, and because it is desirable to keep the model insensitive to c_N and c_P at this stage. The C cost of fungal nutrient uptake is not commonly reported in the literature and probably varies with environmental conditions. For example, (Hobbie and Högberg, 2012) found c_N ranges from 0-180 g C g N⁻¹ based on isotopic theoretical calculations. They further suggest that as the environment becomes more N-abundant, the fungi allow a greater fraction of their assimilated N to be transferred to the plant, resulting in a decline in the C cost.

$$C_{pre,N,myc,j} = c_N \left(N_{pre,myc,org,i,j} + N_{pre,myc,inorg,j} \right)$$
 (S25)

$$N_{myc,org,j} = N_{pre,myc,org,j} \min\left(\frac{C_{pre,N,myc,j}}{0.5C_{net,j}}, 1\right)$$
 (S26)

$$N_{myc,org,i,j} = N_{pre,myc,org,i,j} \min \left(\frac{C_{pre,N,myc,j}}{0.5C_{net,j}}, 1 \right) \quad \forall i$$
 (S27)

$$N_{myc,inorg,j} = N_{pre,myc,inorg,j} \min \left(\frac{C_{pre,N,myc,j}}{0.5C_{net,j}}, 1 \right)$$
 (S28)

$$N_{myc,inorg,i,j} = N_{pre,myc,inorg,i,j} \min \left(\frac{C_{pre,N,myc,j}}{0.5C_{net,j}}, 1 \right) \quad \forall j$$
 (S29)

$$C_{myc,j} = \max \left(c_N \left(N_{myc,org,j} + F_{Nlimit} N_{myc,inorg,j} \right), c_P \left(P_{myc,org,j} + F_{Plimit} P_{myc,inorg,j} \right) \right)$$
(S30)

 $C_{pre,N,myc,j}$ – pre-adjustment C cost of N acquisition from inorganic and organic sources via mycorrhizal roots to a PFT, g C m⁻² s⁻¹

 c_N – C cost per unit acquired N via my corrhizal foots, g C g N⁻¹, c_N = 20; for P, c_P = 200

 $N_{myc,org,j}$ – adjusted total rate of N acquisition from organic sources over all the soil layers via mycorrhizal roots, g N m⁻² s⁻¹

 $N_{myc,org,i,j}$ – adjusted rate of N acquisition from organic sources in one soil layer via mycorrhizal roots, g N m⁻² s⁻¹ $N_{myc,inorg,i,j}$ – adjusted total rate of inorganic N acquisition over all the soil layers via mycorrhizal roots, g N m⁻² s⁻¹ $N_{myc,inorg,i,j}$ – adjusted rate of inorganic N acquisition from one soil layer via mycorrhizal roots, g N m⁻² s⁻¹ $C_{myc,j}$ – C cost of nutrient acquisition via mycorrhizal roots to a PFT, g C m⁻² s⁻¹

1.1.9 Reduction of soil organic N content due to the acquisition of mycorrhizal roots

To model the reduction in soil organic N content due to the acquisition by mycorrhizal roots, we distribute the final adjusted organic N acquisition, Eq. (S26), summed over all the vascular PFTs, across the three accessed litter pools proportional to pool size, see Eq. (S31). The organic C in those pools are not changed.

$$\Delta O_{N,i,h} = \begin{cases} -N_{myc,org,i,j} \frac{O_{N,i,h}}{O_{N,i,lab} + O_{N,i,cel} + O_{N,i,lig}} \Delta t & \forall h \in \{lab, cel, lig\} \\ O_{N,i,h} + O_{N,i,cel} + O_{N,i,lig} \Delta t & \forall h \in \{lab, cel, lig\} \\ -N_{myc,org,i,j} \frac{O_{N,i,h}}{O_{N,i,lab} + O_{N,i,cel}} \Delta t & \forall h \in \{lab, cel\} \\ & \text{if } j = \text{shrub} \end{cases}$$
(S31)

 $\Delta O_{N,i,h}$ – change in the size of the plant litter pool in one soil layer in one time step, g N m⁻²

1.1.10 Direct uptake of inorganic nutrients by uncolonized fine roots

In modelling direct fine-root uptake of inorganic nutrients, we included a root surface area term, Eq. (S32), from the PEATBOG model (Wu and Blodau, 2013). The term is related to measurable root economic traits, here radius and density (Bergmann et al., 2020), enabling distinction between the thinner shrub roots and the coarser tree roots at the SPRUCE site (Iversen et al., 2018). We parameterize the fine-root radius and density directly using the observed values at the SPRUCE site for first- and second-order fine roots, which are primarily responsible for the adsorptive function (Iversen et al., 2017; McCormack et al., 2015). The other multipliers in the uptake rate formula parallel those of inorganic N acquisition via mycorrhizal roots, except for the absence of the NSC multiplier, see Eq. (S33) and Eq. (S23). We use the same half-saturation point, $k_{N,j}$, for PATH^{root} and PATH^{myc,inorg} (Eq. (S22)), in order to limit model complexity in the presence of high observational uncertainty (Table S7). The uptake rates are modelled for each soil layer and summed up, Eq. (S34).

$$A_{froot,i,j} = \frac{0.01C_{froot,i}F_{froot,i,j}}{r_j^2 \rho_j}$$
 (S32)

$N_{froot,i,j} = v_{N,froot,j} (1 - M_{myc,j}) A_{froot,i,j} \mathcal{F}_{j} (N_{conc,i}) \mathcal{F}(T_{soi,i}) \mathcal{F}(\Theta_{soi,i}) \mathcal{F}(F_{Nlimit,j})$	(S33)
$N_{froot,j} = \sum_{i=1}^{10} N_{froot,i,j}$	(S34)

 $A_{froot,i,j}$ – total surface area of fine roots in one soil layer, cm² m⁻²

 r_i – fine-root radius of the PFT, cm

 ρ_i – fine-root density of the PFT, g C cm⁻³

 $v_{N,froot,j}$ – maximum fine-root inorganic N uptake rate per unit uncolonized root surface area, g N cm $^{-2}$ s $^{-1}$

1.2 Removal of pretreatment variability

For each variable among AGNPP_{spruce}, AGNPP_{tamarack}, annual maximum LAI of spruce, and annual maximum LAI of tamarack, we fit an ordinary least-squares regression:

$$X^{post} \sim I(CO_2) + T_{air} + Year + X^{pre} + I(CO_2) \times T_{air} + I(CO_2) \times Year$$
 (S35)

, where X^{post} is the post-treatment value in a year and enclosure, $I(CO_2)$ indicates whether that enclosure is treated with elevated CO_2 ($I(CO_2)=1$) or not ($I(CO_2)=0$), T_{air} is the annual mean air temperature in the year and enclosure, X^{pre} is the observed year 2014 pre-treatment value in the enclosure. After fitting this initial formula, we drop all the insignificant terms using $p \le 0.05$ criteria and re-fit a final regression. If the pretreatment term is still significant in the final regression, we remove its effect as $X^{adj} = X^{post} - b(X^{pre} - \bar{X}^{pre})$, where b is the regression coefficient of X^{pre} , \bar{X}^{pre} is the average pre-treatment value across all enclosure, and X^{adj} is the adjusted observed value.

2 Supplementary Tables

Table S2. Biogeochemistry-related parameters in ELM-OLD that are updated in this study using observed or manually tuned values.

Parameter name (Unit)	Explanation	Plant functional type	Values	Source	
leaf_long (year)	leaf longevity for evergreen leaves	Spruce	5	(Salmon et al., 2021)	
		Spruce	35		
froot_cn (gC gN ⁻¹)	Fine root C:N ratio	Tamarack	40	(Iversen et al., 2021)	
		Shrub	55		
		Spruce	90		
livewd_cn (gC gN ⁻¹)	Live wood C:N ratio	Tamarack	60		
		Shrub	85	(Phillips et al., 2017)	
loof on (gC gD-1)	Leaf C:P ratio	Spruce	655.78		
leaf_cp (gC gP-1)	Leai C.F fatio	Tamarack	655.78		

		Shrub	594.72	
cn_s1 (gC gN-1)	C:N ratio of the first SOM pool	-	22	(Griffiths et al., 2017)
cn_s2 (gC gN ⁻¹)	C:N ratio of the second SOM matter pool	-	22	(Griffiths et al., 2017)
cn_s3 (gC gN ⁻¹)	C:N ratio of the third SOM matter pool	-	20	(Griffiths et al., 2017)
cn_s4 (gC gN ⁻¹)	C:N ratio of the fourth SOM pool	-	20	(Griffiths et al., 2017)
		Spruce	0.2	Manually tuned to
r_mort (year ⁻¹)	Whole-plant turnover rate	Tamarack	0.2	match observed
		Shrub	0.12	biomass magnitude

Table S3. Biogeochemistry-related preexisting parameters in ELM-OLD that are optimized. The upper and lower bounds are determined based on previous ranges (Griffiths et al., 2017; Meng et al., 2021; Ricciuto et al., 2018).

Parameter name		Plant		Optimized
in ELMv2-	Explanation	functional	Range	values in ELM-
SPRUCE (Unit)		type		OLDoptim
	Ball-Berry slope of conductance-	Spruce		10.26
mbbopt (1)	photosynthesis relationship, unstressed	Tamarack	[4.5, 13.5]	9.96
	photosynthesis relationship, unsuessed	Shrub		11.33
		Spruce	[191000,	197844
vemaxhd (J mol ⁻¹)	Deactivation energy for Vcmax	Tamarack	210000]	206246
		Shrub	210000]	197588
		Spruce		0.08376
flnr (1)	Fraction of leaf N in in Rubisco enzyme	Tamarack	[0.05, 0.30]	0.19381
		Shrub		0.29826
	Specific leaf area at top of canopy	Spruce	[0.0051,	0.00909
		Бргасс	0.0095]	0.00707
slatop (m ² gC ⁻¹)		Tamarack	[0.01708,	0.02572
similar (iii ge)		Turraraen	0.02604]	
		Shrub	[0.01666,	0.01985
		Sinuo	0.0308]	0.01703
br_mr_pft (gC gN-		Spruce	[10-6, 5*10-	3.283*10-6
1 s ⁻¹)	Base rate of maintenance respiration	Tamarack	6]	1.319*10-6
		Shrub] ,	4.234*10 ⁻⁶
q10 mr pft (1)	Q ₁₀ of maintenance respiration	Spruce	[1.2, 3.8]	2.322
410_IIII_pit (1)	Viv of maintenance respiration	Tamarack	[1.2, 3.0]	3.209

		Shrub		1.369
froot leaf (gC gC		Spruce		1.015
noot_lear (ge ge	Ratio of fine root to leaf allocation	Tamarack	[0.3, 1.3]	1.085
,		Shrub		0.628
stem leaf (n/a)	Parameter controlling stem-to-leaf	Spruce	[-0.5, -0.1]	-0.4796
stem_lear (ii/a)	allocation ratio	Tamarack	[0.5, 0.1]	-0.3084
decomp_depth_	e-folding depth for reduction in	_	[0.3, 1.0]	0.3039
efolding (m)	decomposition		[0.5, 1.0]	0.3037
q10_hr (1)	Q ₁₀ for heterotrophic respiration	-	[1.4, 2.5]	1.922
mino2lim (1)	Minimum anaerobic decomposition rate	_	[0.0001,	0.003131
(1)	as a fraction of potential aerobic rate		0.05]	0.000101

 $\label{thm:constraint} \textbf{Table S4. Newly added parameters in ELM-MYCI that are manually tuned.}$

Symbol (Unit)	Equation appeared in	Plant functional type	Value	Range in one-at- a-time sensitivity analysis	Source
		Spruce	0.7		Manually tuned based on
$a_j(1)$	Eq. (S12)	Tamarack	0.5	[0.2, 0.8]	observed ranges (Rossi et al., 2012; Xie et al., 2021)
θ_{opt} (1)	Eq. (S14)	-	0.6	[0.3, 0.9]	(Frolking et al., 2002)
α(1)	Eq. (S15)	-	1.5	[0.75, 2.25]	Selected based on comparing a range of values in Figure S3
k_{nsc} (1)	Eq. (S16)	-	2	[1, 3]	Manually tuned
		Spruce	11.7605	-	
a_{root} (1)	Eq. (S18)	Tamarack	11.7605	-	Fitted to observed fine
		Shrub	7.5535	-	root depth distribution at
		Spruce	-0.11713	-	SPRUCE (Weber et al.,
b_{root} (1)	Eq. (S18)	Tamarack	-0.11713	-	2025)
		Shrub	0.04493	-	
$u_{N,fungi,j}$ $(gN gC^{-1})$	Fa (\$17)	Tamarack	1.0209*10 ⁻⁸	[1.0209*10 ⁻⁹ , 1.0209*10 ⁻⁷]	Manually tuned to ensure
$\left(\frac{gN}{s^{-1}}\right)$	Eq. (S17)	Shrub	3.5748 *10-8	[3.5748*10 ⁻⁹ , 3.5748*10 ⁻⁷]	all PFTs grow

		Spruce	7		Manually tuned to
$k_{N,j}$ (gN	E (C22)	Tamarack	7	[2.5.14]	approximately match
m ⁻³)	Eq. (S22)	G1 1		[3.5, 14]	annual average simulated
		Shrub	7		soil inorganic N levels
	Dhoomhomia	Tamarack	0.004955		Manually tuned to
$k_{P,j}$ (gP	Phosphorus counterpart of Eq.			[0.002478,	approximately match
m ⁻³)	(S22)	Shrub	0.004955	0.009911]	annual average simulated
	(322)				soil inorganic P levels
12		Spruce	4.5977*10-9	[4.5977*10 ⁻¹⁰ ,	
$v_{N,fungi,j}$ $(gN gC^{-1})$	Eq. (S23)	Spruce	4.3977 10	4.5977*10 ⁻⁸]	
(gIV gC)	Eq. (323)	Shrub	3.3289*10-9	[3.3289*10 ⁻¹⁰ ,	Manually tuned with
8)		Siliuo	3.3289 10	3.3289*10-8]	reference to values in (He
12	Phosphorus	Tamarack	2.7566*10 ⁻¹⁰	[2.7567*10 ⁻¹¹ ,	et al., 2021; Shao et al.,
$v_{P,fungi,j}$	counterpart of Eq.	Tamarack	2./366*10	2.7567*10-9]	2023)
(gP gC ⁻¹ s ⁻¹)	(S23)	Shrub	8.0369*10 ⁻¹⁰	[8.0369*10 ⁻¹¹ ,	
')		Silluo		8.0369*10-9]	
					Manually tuned in line
c_P (gC	Phosphorus counterpart of Eq. (S25), Eq. (S30)	-	200	[100, 1000]	with the typical order-of-
gP^{-1}					magnitude N:P ratio
51)					(~10:1) in soil-plant
					systems
		Spruce	0.012	-	Unpublished observed
r_j (cm)	Eq. (S32)	Tamarack	0.018	-	data (Iversen et al., 2018)
		Shrub	0.0045	-	uma (1 · 415 611 6 · mi, 2 · 1 · 6)
		Spruce	0.16	-	Unpublished observed
ρ_j (gC	Eq. (S32)	Tamarack	0.15 gC cm ⁻³	-	data, assuming 46% C in
cm ⁻³)	24. (222)	Shrub	0.09 gC cm ⁻³	_	biomass (Iversen et al.,
		2111 010	ovos go om		2018)
$v_{N,froot,j}$					Manually tuned with
(gN gC ⁻¹	Eq. (S33)	Spruce	4.2538*10 ⁻¹²	[4.2538*10 ⁻¹³ ,	reference to values in
(\mathbf{s}^{-1})	гч. (633)	1 -		4.2538*10 ⁻¹¹]	(Shao et al., 2023; Wu
- /					and Blodau, 2013)

Table S5. Newly added parameters in ELM-MYCI that are optimized.

Symbol	Equation appeared in	Plant	Range	Optimized valu	es
Symbol	Equation appear ou in	functional type	rumge	ELM-MYCI	ELM-MYCI _{optim}

$a_{j}(1)$	Eq. (S12)	Shrub	[0.2, 0.8]	0.9053	0.6868
		Spruce	[-0.1, 0.1]	-0.07366	-0.09000
$b_{j}(1)$	Eq. (S12)	Tamarack [-0.1, 0.1]		0.00576	-0.06763
		Shrub	[-0.1, 0]	-0.07368	-0.06777
$q_{10}(1)$	Eq. (S13)	-	[1, 4]	3	1
$u_{N,fungi,j}$ (gN gC ⁻¹ s ⁻¹)	Eq. (S17)	Spruce	[2.55*10 ⁻¹⁰ , 2.55*10 ⁻⁸]	2.4368*10 ⁻⁸	1.9289*10 ⁻⁸
11 ₂ c	Phosphorus	Spruce	[1.520*10 ⁻¹² , 1.520*10 ⁻¹⁰]	6.9176*10 ⁻¹¹	2.749*10 ⁻¹¹
$ \begin{array}{c} u_{P,fungi,j} \\ (\text{gN gC}^{-1} \text{ s}^{-1}) \end{array} $	counterpart of Eq. (S17)	Tamarack	[1.079*10 ⁻¹¹ , 1.079*10 ⁻⁹]	8.1831*10 ⁻¹⁰	7.782*10 ⁻¹⁰
,	(\$17)	Shrub	[1.127*10 ⁻¹¹ , 1.127*10 ⁻⁹]	1.4757*10 ⁻¹⁰	2.427*10 ⁻¹¹
$k_{P,j}$ (gP m ⁻³)	Phosphorus counterpart of Eq. (S22)	Spruce	[0.002478, 0.009911]	0.004457	0.009172
$v_{N,fungi,j}$ (gN gC ⁻¹ s ⁻¹)	Eq. (S23)	Tamarack	[3.4833*10 ⁻⁹ , 3.4833*10 ⁻⁷]	8.7018*10 ⁻⁹	2.7459*10 ⁻⁷
$v_{P,fungi,j}$ (gP gC ⁻¹ s ⁻¹)	Phosphorus counterpart of Eq. (S23)	Spruce	[1.2229*10 ⁻¹¹ , 1.2229*10 ⁻⁹]	1.8946*10 ⁻¹¹	8.2067*10 ⁻¹⁰
c_N (gC gN-1)	Eq. (S25), (S30)	-	[10, 100]	34	32
$v_{N,froot,j}$	Eq. (\$33)	Tamarack	[9.6838*10 ⁻¹² , 9.6838*10 ⁻¹⁰]	8.5323*10 ⁻¹⁰	3.4772*10 ⁻¹⁰
(gN gC ⁻¹ s ⁻¹)	Eq. (S33)	Shrub	[9.6462*10 ⁻¹³ , 9.6462*10 ⁻¹¹]	2.5154*10 ⁻¹²	2.0811*10-11
12	Phoenhorus	Spruce	[4.4409*10 ⁻¹⁴ , 4.4409*10 ⁻¹²]	2.8185*10-12	3.7779*10 ⁻¹²
$v_{P,froot,j}$ $(\text{gP gC}^{-1} \text{ s}^{-1})$	Phosphorus counterpart of Eq. (\$33)	Tamarack	[3.6461*10 ⁻¹³ , 3.6461*10 ⁻¹¹]	1.1268*10-12	5.9747*10 ⁻¹²
,	(S33)	Shrub	[5.5157*10 ⁻¹⁴ , 5.5157*10 ⁻¹²]	3.2882*10-12	2.2162*10 ⁻¹²

Table S6. Review of experimentally measured uptake rates by fungi-colonized and uncolonized fine roots. If the paper reported a maximum rate constant, that value is used here; otherwise, the fastest measured rate is used. The estimated values in gN or gP $\rm cm^{-2}~s^{-1}$ use Eq. (S32) with 0.015 cm radius and 0.155 gC $\rm cm^{-3}$ density for trees, and 0.0045 cm radius and 0.09 gC $\rm cm^{-3}$ density for shrub and herbs.

Plant species	Nutrient species	Value in original unit	Converted value (gN or gP cm ⁻² s ⁻¹)	Converted value (gN or gP gC ⁻¹ s ⁻¹)	Source	
Picea asperata, uncolonized roots	NH_4^+	130 pmol cm ⁻² s ⁻¹	1.820*10 ⁻⁹	2.401*10 ⁻⁷		
	NO_3^-	90 pmol cm ⁻² s ⁻¹	1.260*10-9	1.662*10 ⁻⁷	(Xie et al., 2021)	
Picea asperata, EcM	NH_4^+	30 pmol cm ⁻² s ⁻¹	4.200*10 ⁻¹⁰	5.540*10-8		
colonized roots	NO_3^-	20 pmol cm ⁻² s ⁻¹	2.800*10 ⁻¹⁰	3.693*10-8		
Douglas fir, uncolonized	NH_4^+	22 nmol m ⁻² s ⁻¹	3.080*10-11	4.063*10-9		
roots	NO ₃	25 nmol m ⁻² s ⁻¹	3.500*10 ⁻¹¹	4.616*10-9	(Hawkins et al.,	
Lodgepole pine,	NH_4^+	14 nmol m ⁻² s ⁻¹	1.960*10 ⁻¹¹	2.585*10-9	2008)	
uncolonized roots	NO_3^-	20 nmol m ⁻² s ⁻¹	2.800*10-11	3.693*10-9		
Hardwood trees	NH_4^+	8 μmol g root ⁻¹ hr ⁻¹	2.359*10 ⁻¹⁰	3.111*10 ⁻⁸	(Sanders- DeMott et al.,	
Hardwood trees	NO ₃	0.25 μ mol g root ⁻¹ hr ⁻¹	7.371*10 ⁻¹²	9.722*10 ⁻¹⁰	2018)	
Eriophorum vaginatum	NH_4^+	13.7 μmol g ⁻¹ hr ⁻	2.111*10 ⁻¹¹	5.328*10 ⁻⁸	(Chapin et al., 1993)	
Vaccinium macrocarpon, uncolonized roots	NO ₃	0.017 μ mol g ⁻¹ DW min ⁻¹	1.572*10 ⁻¹²	3.967*10 ⁻⁹	(Kosola et al.,	
Vaccinium macrocarpon, ErM colonized roots	NO ₃	0.16 μ mol g ⁻¹ DW min ⁻¹	1.479*10 ⁻¹¹	3.733*10 ⁻⁸	2007)	
Pinus sylvestris, uncolonized	PO ₄ ³⁻	0.2 nmol s ⁻¹ g ⁻¹ d. wt root	4.701*10 ⁻¹¹	6.200*10 ⁻⁹	(Colpaert et al.,	
Pinus sylvestris, colonized whole plant	PO ₄ ³⁻	1 nmol s ⁻¹ g ⁻¹ d. wt root	2.350*10 ⁻¹⁰	3.100*10 ⁻⁸	1999)	
Pinus sylvestris, uncolonized	PO ₄ ³⁻	0.08 nmol g ⁻¹ s ⁻¹	1.880*10 ⁻¹¹	2.480*10-9	(Van Tichelen and Colpaert,	
Pinus sylvestris, colonized whole plant	PO ₄ ³⁻	0.13-0.62 nmol g ⁻¹ s ⁻¹	3.055*10 ⁻¹¹ - 1.457*10 ⁻¹⁰	4.030*10 ⁻⁹ - 1.922*10 ⁻⁸	2000)	

Calluna vulgaris,		1500 ng mg root			(Arndal et al.,
colonized by endophytes	PO_4^{3-}	1500 pg mg root			,
and ErM		FW ⁻¹ hour ⁻¹	1.360*10 ⁻¹³	3.432*10 ⁻¹⁰	2013)

Table S7. Review of experimentally measured half-saturation point in uptake kinetics.

Value in original unit	Converted value (gN m ⁻³ water)	Plant species	Nutrient species	Source	
242 μmol kg ⁻¹	3.338	Eriophorum vaginatum	NH_4^+	(Chapin et al., 1993)	
Only linear relationship observed	-	Vaccinium macrocarpon, uncolonized roots	NH_4^+		
Only linear relationship observed	linear - Waccinium - macrocarpon, uncolonized roots		NO_3^-	(Kosola et al., 2007)	
34.54 μmol kg ⁻¹	0.48	Vaccinium macrocarpon, colonized roots	NH_4^+	(Rosoia et al., 2007)	
17.75 μmol kg ⁻¹	0.25	Vaccinium macrocarpon, ErM colonized roots	NO_3^-		
12.1 μmol kg ⁻¹	0.17	Pinus sylvestris, uncolonized	PO ₄ ³⁻	(Van Tichelen and	
3.5-10.2 μmol kg ⁻¹	0.049-0.143	Pinus sylvestris, colonized whole plant	PO ₄ ³⁻	Colpaert, 2000)	

Table S8. Sphagnum cover (%) by year and treatment chamber (Norby et al., 2019).

Treatment	2016	2017	2018	2019	2020	2021
+0.00	25	24.5	24.9	23.7	24.6	24.6
+2.25	25	21.1	21.1	24	19	19
+4.50	25	19.4	19.3	12.3	9.2	9.2
+6.75	25	21.3	10.1	8.1	4	4
+9.00	24	8.9	3.8	3.6	0.6	0.6
+0.00 CO ₂	25	25	24	23.3	23.3	23.3
+2.25 CO ₂	24.3	17.4	16.5	14.5	14.5	14.5

+4.50 CO ₂	25	4.8	5.7	3.7	1.2	1.2
+6.75 CO ₂	22	12.1	14	10.1	7.1	7.1
+9.00 CO ₂	23.1	11.2	4.2	3.7	1.7	1.7
Ambient	25	25	25	25	25	25

3 Supplementary Figures

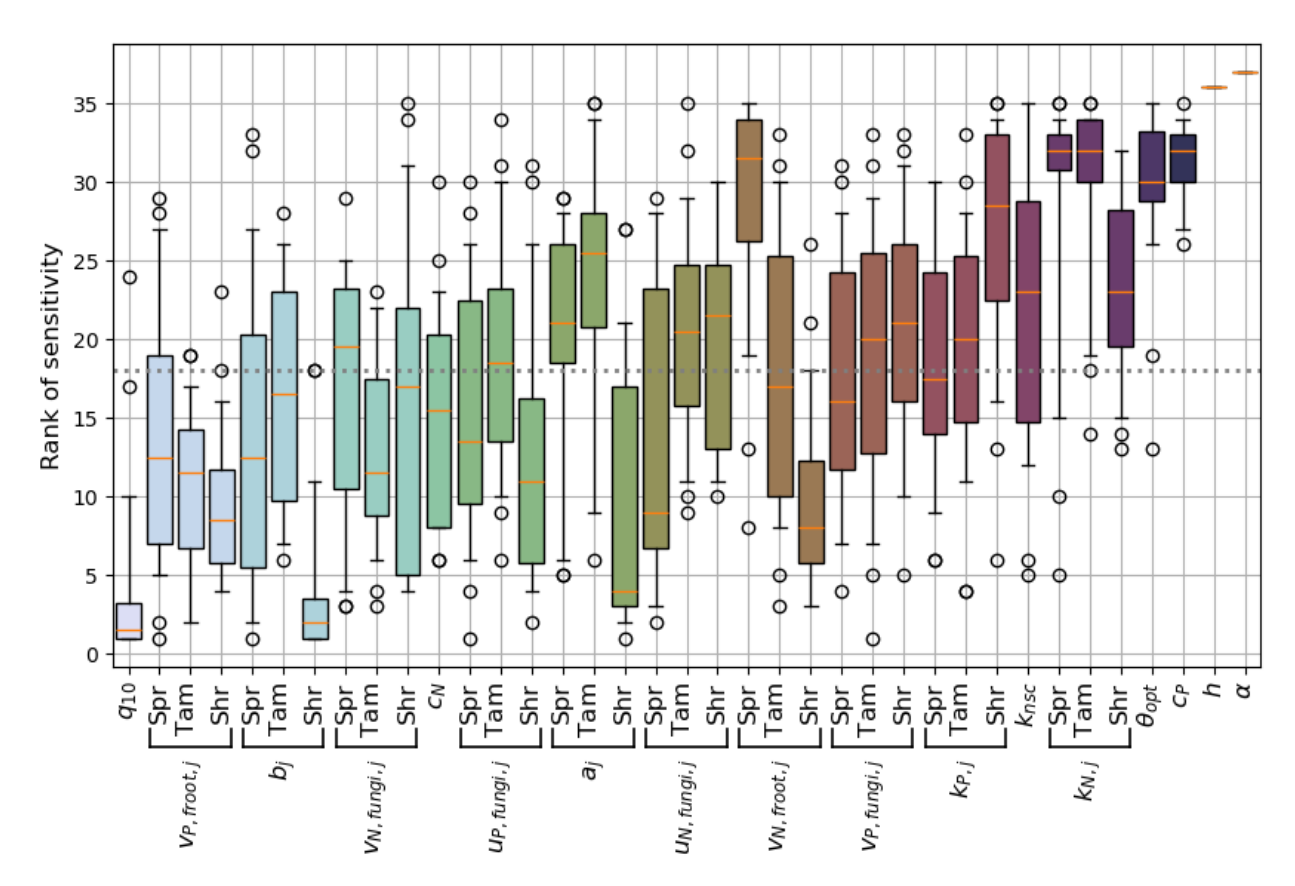


Figure S4. Rank of the sensitivity of carbon fluxes to the newly added parameters in ELM-MYCI. A smaller rank means greater sensitivity. Parameters that have PFT-specific values are grouped together and labelled by Spr – spruce, Tam – tamarack, Shr – shrub. Boxplots show the [min, 5th percentile, 25th percentile, median, 75th percentile, 95th percentile, max] of the ranks across the means and slopes of all the independent carbon flux variables in ambient and elevated CO_2 enclosures. Parameters/PFT-specific values ranked below the threshold line (horizontal, dashed grey) are selected for ensemble simulation and optimization.

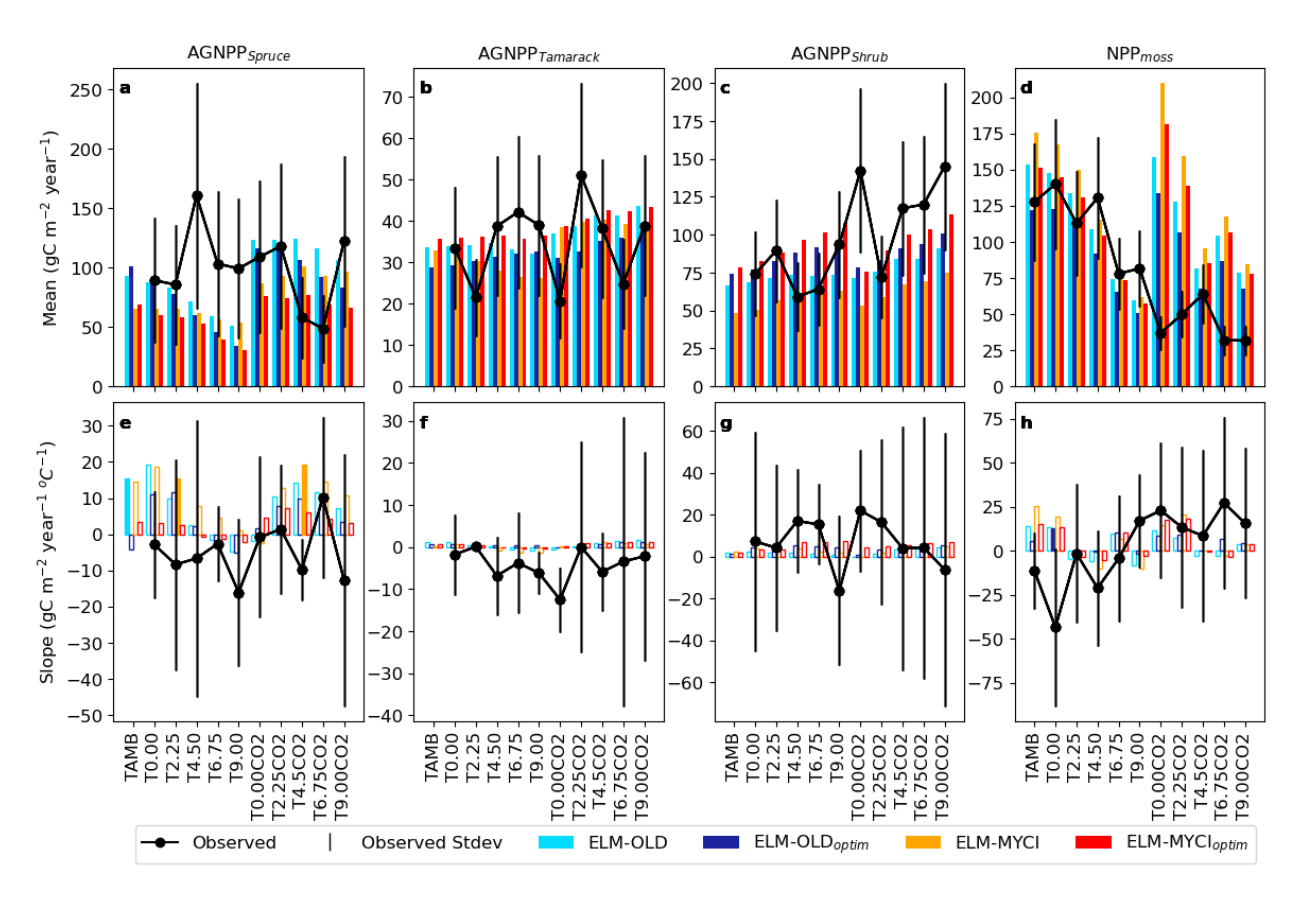


Figure S5. Enclosure-by-enclosure mean and temperature sensitivity of selected C fluxes. The observational uncertainty intervals are estimated in the same manner as Fig. 1 (see main text Sect. 2.4). The modelled slopes have solid bars when they are significant at $p \le 0.05$ (two-sided t-test), and otherwise hollow bars. The modelled values are from the best-performing ensemble members using RAE criteria (main text Eq. (1)).

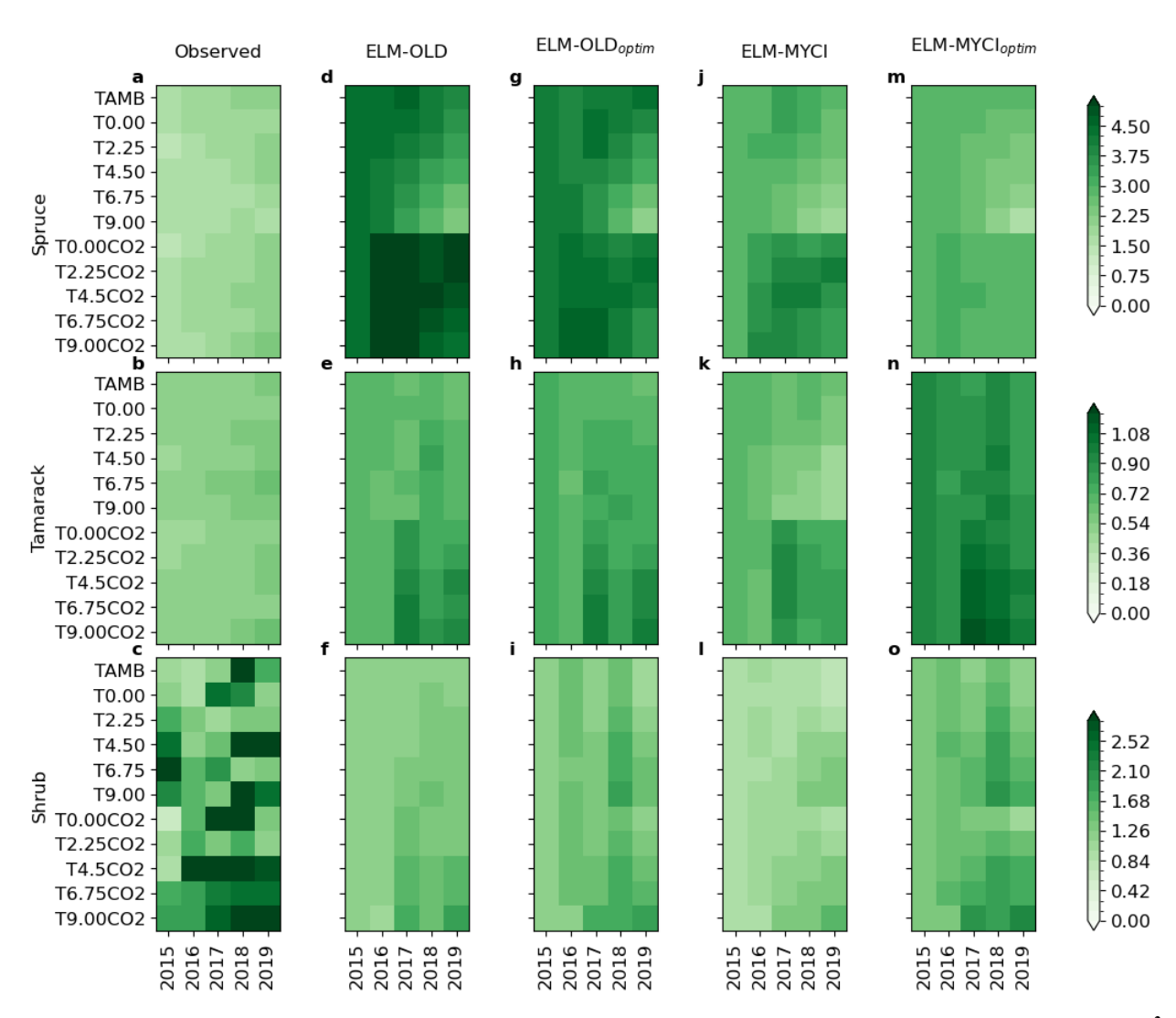


Figure S6. Observed annual maximum leaf area index and the corresponding simulated levels by the four model setups (m² m² ground area).

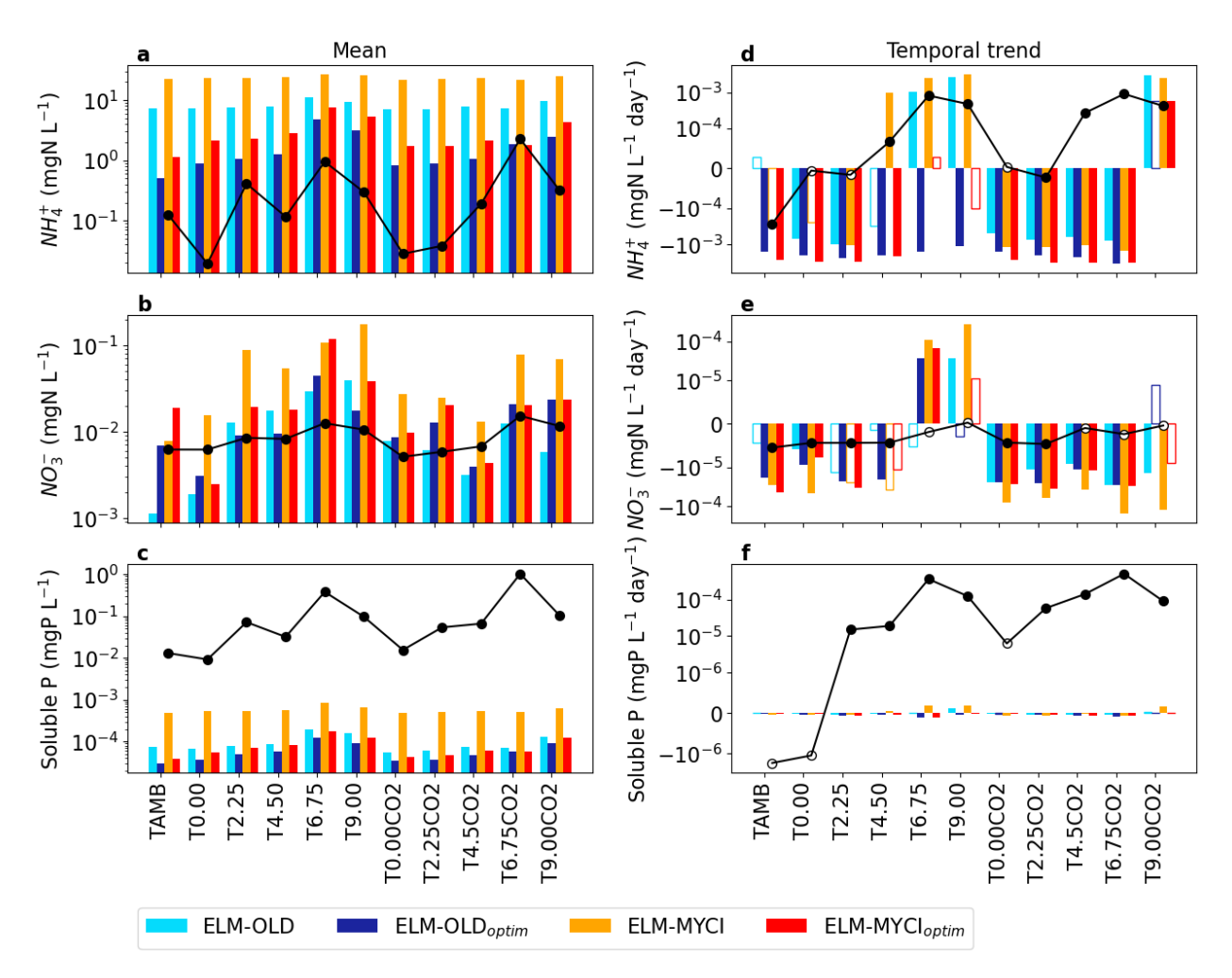


Figure S7. Observed and simulated mean values and least squares linear temporal trends in hollow soil pore water nutrient concentrations at 30cm depth during 2015-2020. Logscale is used because the modeled and observed values differ by orders of magnitudes. For the temporal trends, solid bars mean the trend is significant at $p \le 0.05$ (two-sided t-test) and empty bars means insignificant.

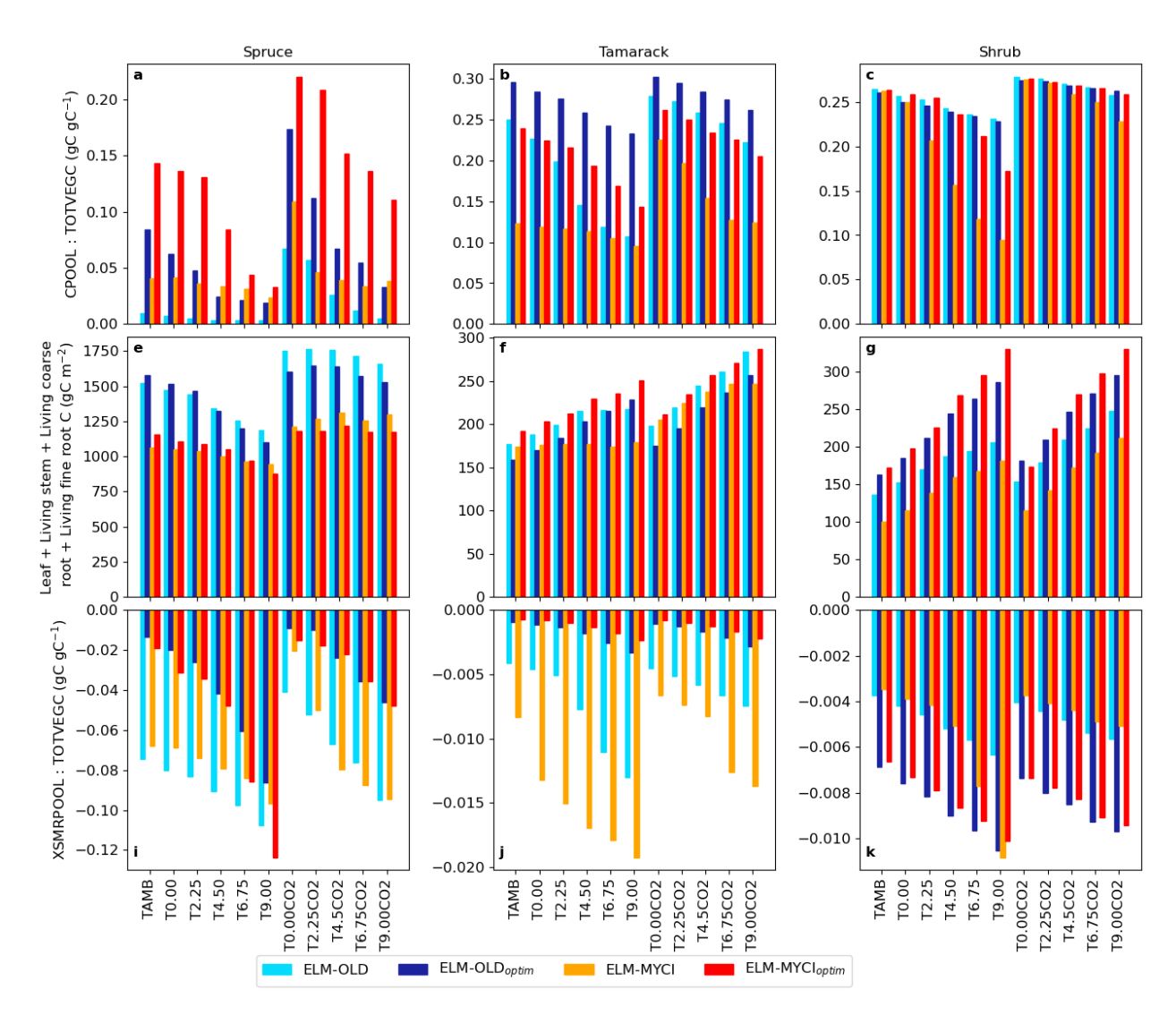


Figure S8. Supplementary diagnostics on simulation results: (a-c) the ratio of nonstructural carbohydrates (CPOOL) to total vegetation biomass (TOTVEGC), (e-g) the total living biomass, which does not include dead stem and dead coarse root part of TOTVEGC, (i-k) the ratio of the virtual XSMR pool to total vegetation biomass. The ratios are calculated from enclosure-wise 2015-2021 averages.

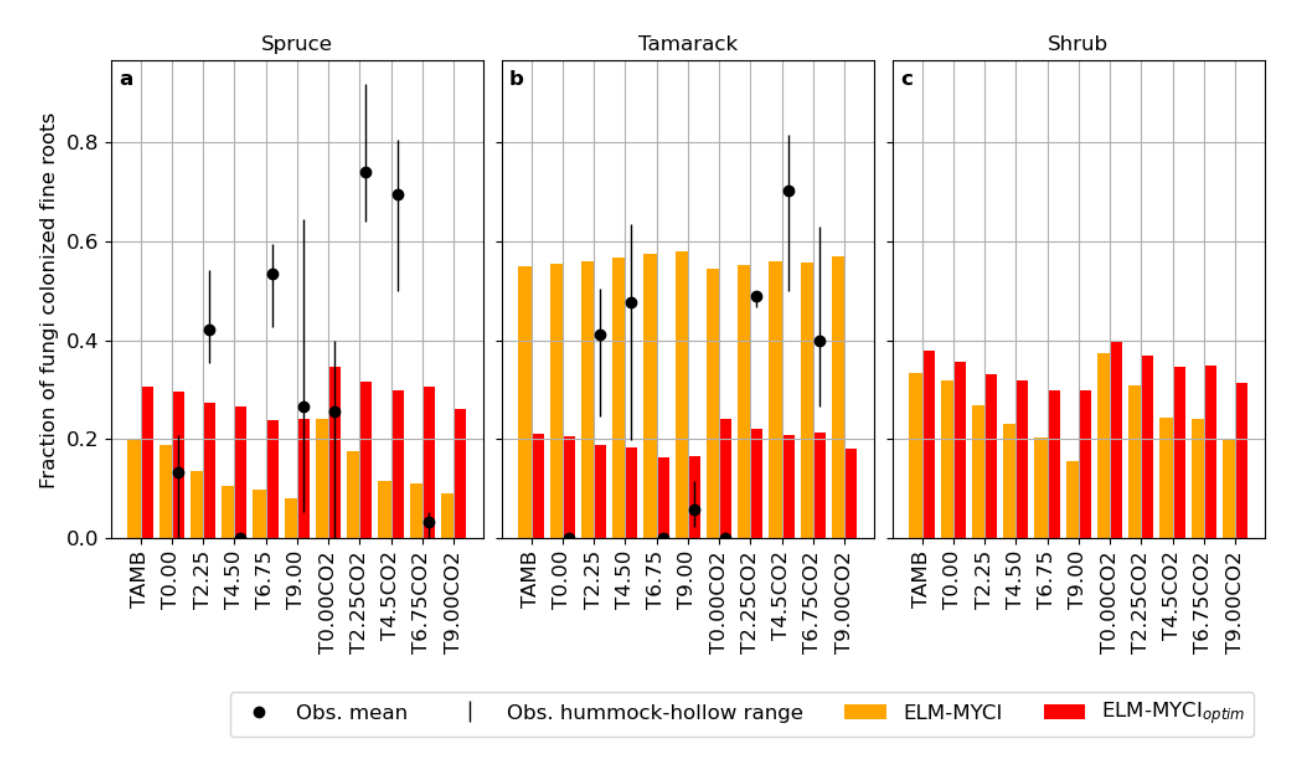


Figure S9. Fraction of fungi-colonized fine roots observed for tamarack in selected enclosures and simulated by the two modified model setups for spruce, tamarack, and shrub in all the enclosures. The observations were made in summer 2017, with one data point from the hummock and one from the hollow (Duchesneau et al., 2024). The display shows their weighted mean $(0.64 \times \text{hummock} + 0.36 \times \text{hollow})$ and the range. The simulated values are averaged over 2015-2021 for each enclosure and use the same hummock-hollow average $(0.64 \times \text{hummock} + 0.36 \times \text{hollow})$ as all the other modelled variables.

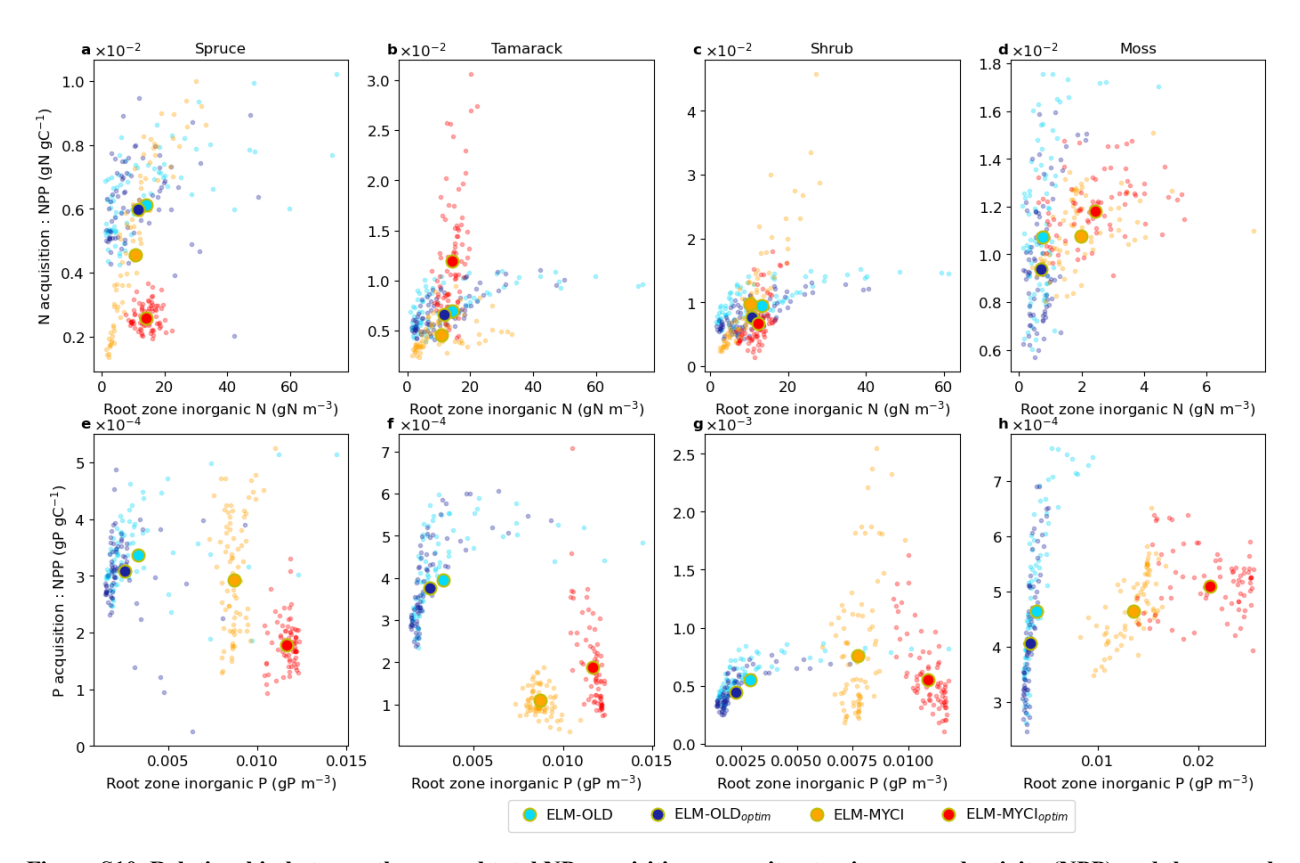


Figure S10. Relationship between the annual total NP acquisition per unit net primary productivity (NPP) and the annual mean soil inorganic nutrient content in different model setups. The total acquisition is equal to inorganic nutrient uptake in ELM-OLD and ELM-OLD $_{\rm optim}$, and equal to the sum of all three pathways (actual inorganic nutrient uptake by uncolonized fine roots, actual inorganic nutrient uptake by mycorrhizal roots) in ELM-MYCI and ELM-MYCI $_{\rm optim}$. We normalize the acquisition to per unit NPP to remove the influences from vegetation biomasses and highlight the differences in the shapes of the relationships. Each small dot represents a single enclosure-year combination, and all the dots together span all the enclosures and 2015-2021. The large dots represent averages over all the years and chambers. The soil inorganic nutrient contents are weighted averages over all the soil layers using the plant functional type's fine-root fractions in each soil layer.

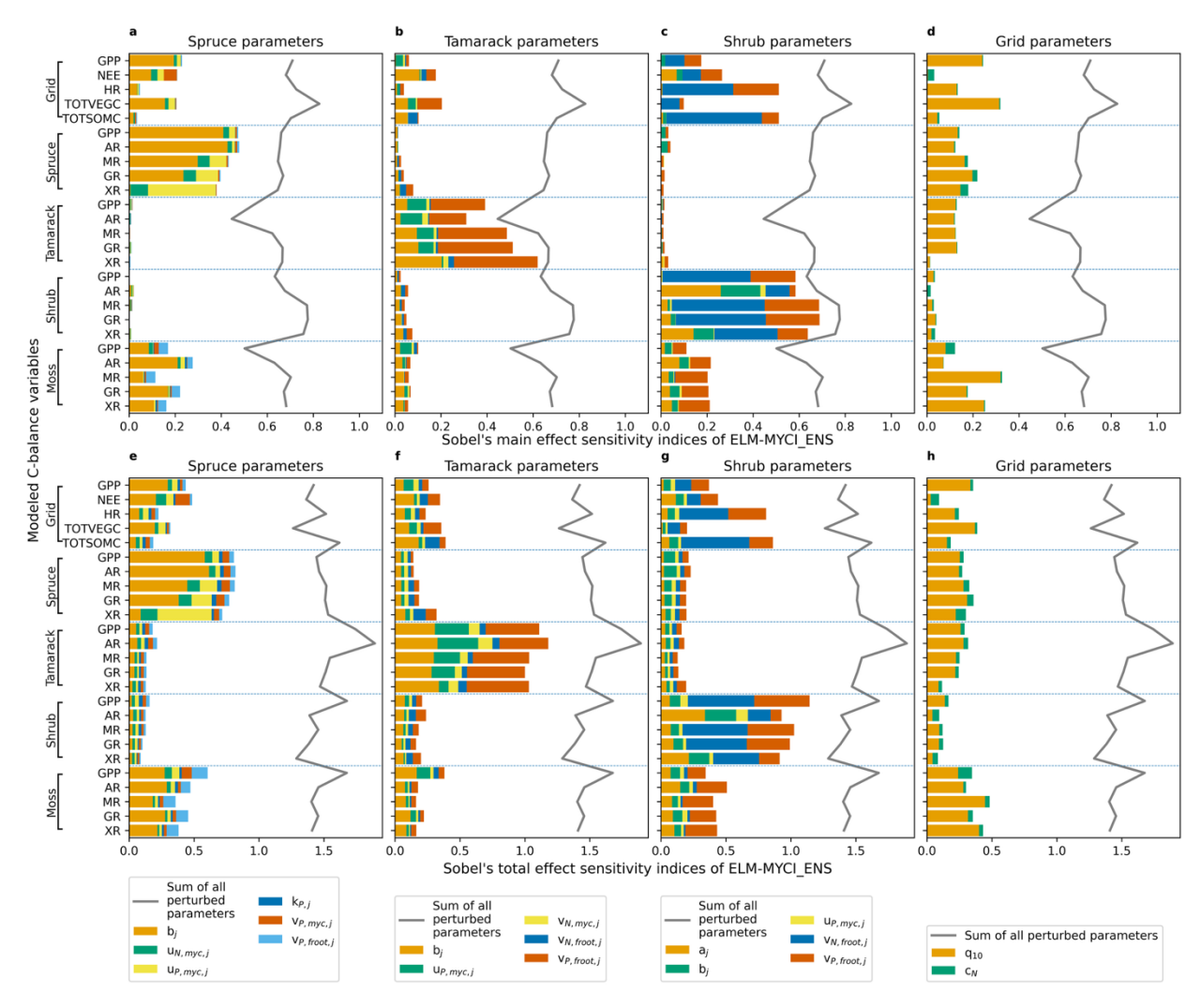


Figure S11. Sobol's main-effect and total-effect sensitivity indices of selected C-balance variables to the newly added model parameters, calculated from ELM-MYCI_ENS. For better display, the indices are partitioned into subpanels according to whether it is a PFT-specific or column-level parameter. Stacking the bars across the four panels in each row gives the sum of the main or total effects over all the perturbed parameters, which are also displayed as a grey line for reference in each panel. The C-balance variables in each panel are grouped according to whether it is a column-level, spruce, tamarack, shrub, or moss variable. Parameter definitions can be found in Table S5 and equations referred therein.

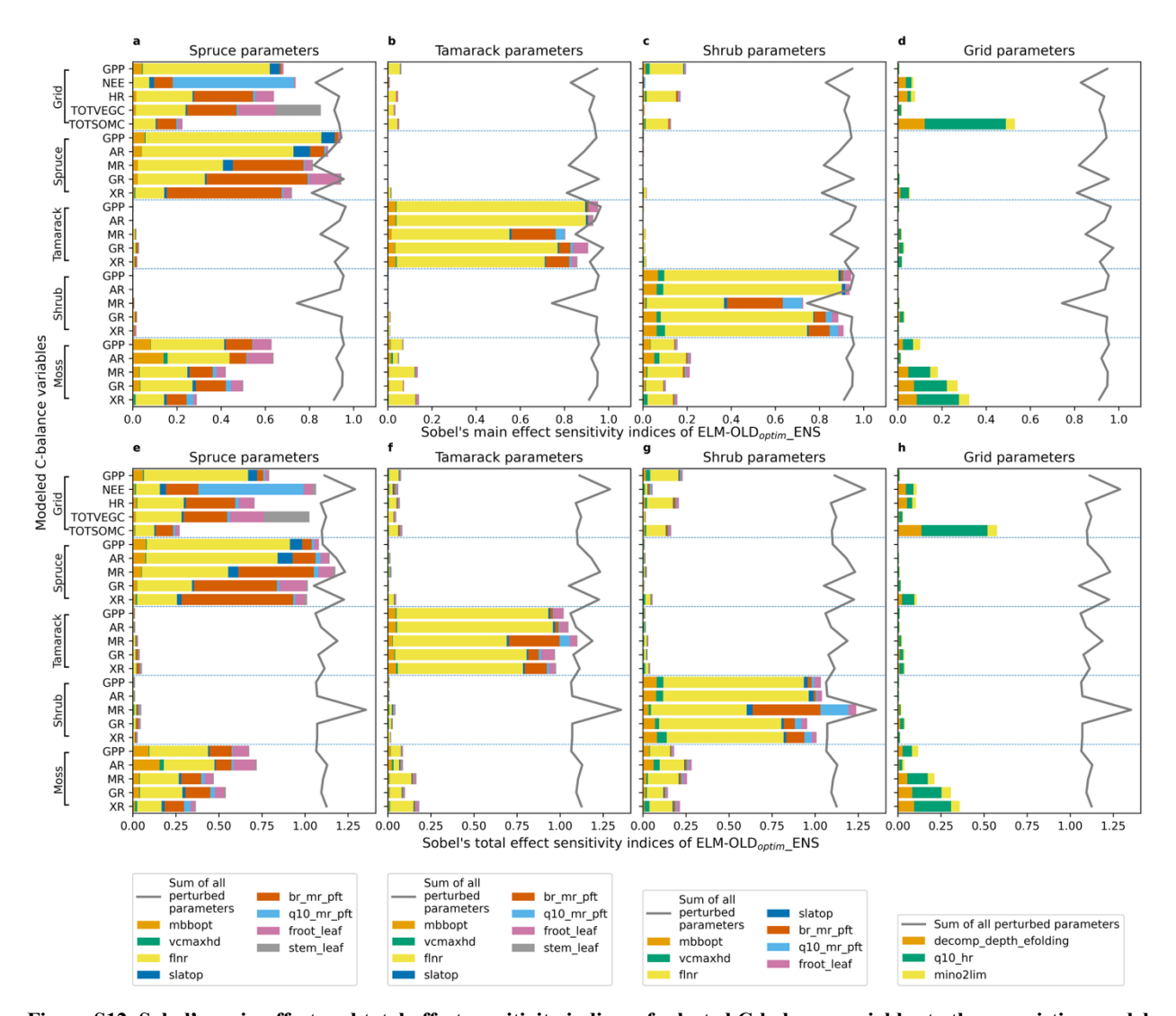


Figure S12. Sobol's main-effect and total-effect sensitivity indices of selected C-balance variables to the preexisting model parameters, calculated from ELM-OLD_{optim}_ENS. For better display, the indices are partitioned into subpanels according to whether it is a PFT-specific or column-level parameter. Stacking the bars across the four panels in each column gives the sum of the main or total effects over all the perturbed parameters, which are also displayed as a grey line for reference in each panel. The C-balance variables in each panel are grouped according to whether it is a column-level, spruce, tamarack, shrub, or moss variable. Parameter definitions can be found in Table S3.

4 References

Arndal, M. F., Merrild, M. P., Michelsen, A., Schmidt, I. K., Mikkelsen, T. N., and Beier, C.: Net root growth and nutrient acquisition in response to predicted climate change in two contrasting heathland species, Plant Soil, 369, 615–629, https://doi.org/10.1007/s11104-013-1601-8, 2013.

Bergmann, J., Weigelt, A., van der Plas, F., Laughlin, D. C., Kuyper, T. W., Guerrero-Ramirez, N., Valverde-Barrantes, O. J., Bruelheide, H., Freschet, G. T., Iversen, C. M., Kattge, J., McCormack, M. L., Meier, I. C., Rillig, M. C., Roumet, C., Semchenko, M., Sweeney, C. J., van Ruijven, J., York, L. M., and Mommer, L.: The fungal collaboration gradient dominates the root economics space in plants, Sci. Adv., 6, eaba3756, https://doi.org/10.1126/sciadv.aba3756, 2020.

Burrows, S. M., Maltrud, M., Yang, X., Zhu, Q., Jeffery, N., Shi, X., Ricciuto, D., Wang, S., Bisht, G., Tang, J., Wolfe, J., Harrop, B. E., Singh, B., Brent, L., Baldwin, S., Zhou, T., Cameron-Smith, P., Keen, N., Collier, N., Xu, M., Hunke, E. C., Elliott, S. M., Turner, A. K., Li, H., Wang, H., Golaz, J. -C., Bond-Lamberty, B., Hoffman, F. M., Riley, W. J., Thornton, P. E., Calvin, K., and Leung, L. R.: The DOE E3SM v1.1 biogeochemistry configuration: Description and simulated ecosystem-climate responses to historical changes in forcing, J. Adv. Model Earth Syst., 12, https://doi.org/10.1029/2019MS001766, 2020.

Chalk, P. and Smith, C.: On inorganic N uptake by vascular plants: Can 15N tracer techniques resolve the NH4+ versus NO3- "preference" conundrum?, European Journal of Soil Science, 72, 1762–1779, https://doi.org/10.1111/ejss.13069, 2021.

Chapin, F. S., Moilanen, L., and Kielland, K.: Preferential use of organic nitrogen for growth by a non-mycorrhizal arctic sedge, Nature, 361, 150–153, https://doi.org/10.1038/361150a0, 1993.

Clemmensen, K. E., Durling, M. B., Michelsen, A., Hallin, S., Finlay, R. D., and Lindahl, B. D.: A tipping point in carbon storage when forest expands into tundra is related to mycorrhizal recycling of nitrogen, Ecology Letters, 24, 1193–1204, https://doi.org/10.1111/ele.13735, 2021.

Colpaert, J. V., Tichelen, K. K. V., Assche, J. a. V., and Laere, A. V.: Short-term phosphorus uptake rates in mycorrhizal and non-mycorrhizal roots of intact Pinus sylvestris seedlings, The New Phytologist, 143, 589–597, https://doi.org/10.1046/j.1469-8137.1999.00471.x, 1999.

Daryanto, S., Wang, L., Gilhooly, W. P., III, and Jacinthe, P.-A.: Nitrogen preference across generations under changing ammonium nitrate ratios, Journal of Plant Ecology, 12, 235–244, https://doi.org/10.1093/jpe/rty014, 2019.

Defrenne, C. E., Childs, J., Fernandez, C. W., Taggart, M., Nettles, W. R., Allen, M. F., Hanson, P. J., and Iversen, C. M.: High-resolution minirhizotrons advance our understanding of root-fungal dynamics in an experimentally warmed peatland, Plants, People, Planet, 3, 640–652, https://doi.org/10.1002/ppp3.10172, 2021.

Duchesneau, K., Defrenne, C., Petro, C., Malhotra, A., Moore, J., Childs, J., Hanson, P., Iversen, C., and Kostka, J.: SPRUCE Root Tip and Ectomycorrhizal Fungi Colonization Measurements from Ingrowth Cores, 2017, https://doi.org/10.25581/SPRUCE.119/2476173, 2024.

Forsmark, B., Nordin, A., Rosenstock, N. P., Wallander, H., and Gundale, M. J.: Anthropogenic nitrogen enrichment increased the efficiency of belowground biomass production in a boreal forest, Soil Biology and Biochemistry, 155, 108154, https://doi.org/10.1016/j.soilbio.2021.108154, 2021.

Frolking, S., Roulet, N. T., Moore, T. R., Lafleur, P. M., Bubier, J. L., and Crill, P. M.: Modeling seasonal to annual carbon balance of Mer Bleue Bog, Ontario, Canada, Global Biogeochemical Cycles, 16, 4-1-4–21, https://doi.org/10.1029/2001GB001457, 2002.

- Glass, A. D. M., Britto, D. T., Kaiser, B. N., Kinghorn, J. R., Kronzucker, H. J., Kumar, A., Okamoto, M., Rawat, S., Siddiqi, M. Y., Unkles, S. E., and Vidmar, J. J.: The regulation of nitrate and ammonium transport systems in plants, Journal of Experimental Botany, 53, 855–864, https://doi.org/10.1093/jexbot/53.370.855, 2002.
- Griffiths, N. A., Hanson, P. J., Ricciuto, D. M., Iversen, C. M., Jensen, A. M., Malhotra, A., McFarlane, K. J., Norby, R. J., Sargsyan, K., Sebestyen, S. D., Shi, X., Walker, A. P., Ward, E. J., Warren, J. M., and Weston, D. J.: Temporal and Spatial Variation in Peatland Carbon Cycling and Implications for Interpreting Responses of an Ecosystem-Scale Warming Experiment, Soil Science Society of America Journal, 81, 1668–1688, https://doi.org/10.2136/sssaj2016.12.0422, 2017.
- Hawkins, B. J., Boukcim, H., and Plassard, C.: A comparison of ammonium, nitrate and proton net fluxes along seedling roots of Douglas-fir and lodgepole pine grown and measured with different inorganic nitrogen sources, Plant, Cell & Environment, 31, 278–287, https://doi.org/10.1111/j.1365-3040.2007.01760.x, 2008.
- Hawkins, H.-J., Cargill, R. I. M., Van Nuland, M. E., Hagen, S. C., Field, K. J., Sheldrake, M., Soudzilovskaia, N. A., and Kiers, E. T.: Mycorrhizal mycelium as a global carbon pool, Current Biology, 33, R560–R573, https://doi.org/10.1016/j.cub.2023.02.027, 2023.
- He, H., Meyer, A., Jansson, P.-E., Svensson, M., Rütting, T., and Klemedtsson, L.: Simulating ectomycorrhiza in boreal forests: implementing ectomycorrhizal fungi model MYCOFON in CoupModel (v5), Geoscientific Model Development, 11, 725–751, https://doi.org/10.5194/gmd-11-725-2018, 2018.
- He, H., Jansson, P.-E., and Gärdenäs, A. I.: CoupModel (v6.0): an ecosystem model for coupled phosphorus, nitrogen, and carbon dynamics evaluated against empirical data from a climatic and fertility gradient in Sweden, Geoscientific Model Development, 14, 735–761, https://doi.org/10.5194/gmd-14-735-2021, 2021.
- Hobbie, E. A. and Högberg, P.: Nitrogen isotopes link mycorrhizal fungi and plants to nitrogen dynamics, New Phytologist, 196, 367–382, https://doi.org/10.1111/j.1469-8137.2012.04300.x, 2012.
- Högberg, M. N., Briones, M. J. I., Keel, S. G., Metcalfe, D. B., Campbell, C., Midwood, A. J., Thornton, B., Hurry, V., Linder, S., Näsholm, T., and Högberg, P.: Quantification of effects of season and nitrogen supply on tree belowground carbon transfer to ectomycorrhizal fungi and other soil organisms in a boreal pine forest, New Phytologist, 187, 485–493, https://doi.org/10.1111/j.1469-8137.2010.03274.x, 2010.
- Iversen, C. M., McCormack, M. L., Powell, A. S., Blackwood, C. B., Freschet, G. T., Kattge, J., Roumet, C., Stover, D. B., Soudzilovskaia, N. A., Valverde-Barrantes, O. J., Van Bodegom, P. M., and Violle, C.: A global Fine-Root Ecology Database to address below-ground challenges in plant ecology, New Phytologist, 215, 15–26, https://doi.org/10.1111/nph.14486, 2017.
- Iversen, C. M., Childs, J., Norby, R. J., Ontl, T. A., Kolka, R. K., Brice, D. J., McFarlane, K. J., and Hanson, P. J.: Fine-root growth in a forested bog is seasonally dynamic, but shallowly distributed in nutrient-poor peat, Plant Soil, 424, 123–143, https://doi.org/10.1007/s11104-017-3231-z, 2018.
- Iversen, C. M., Brice, D. J., Childs, J., Vander Stel, H. M., and Salmon, V. G.: SPRUCE S1 bog production of newlygrown fine roots assessed using root ingrowth cores in 2013, https://doi.org/10.25581/spruce.091/1782483, 2021.
- Kosola, K. R., Workmaster, B. A. A., and Spada, P. A.: Inoculation of cranberry (*Vaccinium macrocarpon*) with the ericoid mycorrhizal fungus *Rhizoscyphus ericae* increases nitrate influx, New Phytologist, 176, 184–196, https://doi.org/10.1111/j.1469-8137.2007.02149.x, 2007.
- Malhotra, A., Brice, D. J., Childs, J., Graham, J. D., Hobbie, E. A., Vander Stel, H., Feron, S. C., Hanson, P. J., and Iversen, C. M.: Peatland warming strongly increases fine-root growth, Proc. Natl. Acad. Sci. U.S.A., 117, 17627–17634, https://doi.org/10.1073/pnas.2003361117, 2020.

- McCormack, M. L., Dickie, I. A., Eissenstat, D. M., Fahey, T. J., Fernandez, C. W., Guo, D., Helmisaari, H., Hobbie, E. A., Iversen, C. M., Jackson, R. B., Leppälammi-Kujansuu, J., Norby, R. J., Phillips, R. P., Pregitzer, K. S., Pritchard, S. G., Rewald, B., and Zadworny, M.: Redefining fine roots improves understanding of below-ground contributions to terrestrial biosphere processes, New Phytologist, 207, 505–518, https://doi.org/10.1111/nph.13363, 2015.
- Meng, L., Mao, J., Ricciuto, D. M., Shi, X., Richardson, A. D., Hanson, P. J., Warren, J. M., Zhou, Y., Li, X., Zhang, L., and Schädel, C.: Evaluation and modification of ELM seasonal deciduous phenology against observations in a southern boreal peatland forest, Agric. For. Meteorol., 308–309, 108556, https://doi.org/10.1016/j.agrformet.2021.108556, 2021.
- Norby, R. J., Childs, J., Hanson, P. J., and Warren, J. M.: Rapid loss of an ecosystem engineer: *Sphagnum* decline in an experimentally warmed bog, Ecology and Evolution, 9, 12571–12585, https://doi.org/10.1002/ece3.5722, 2019.
- Oleson, K. W., Lawrence, D. M., Bonan, G. B., Drewniak, B., Huang, M., Levis, S., Li, F., Riley, W. J., Swenson, S. C., Thornton, P. E., Bozbiyik, A., Fisher, R., Heald, C. L., Kluzek, E., Lamarque, F., Lawrence, P. J., Leung, L. R., Muszala, S., Ricciuto, D. M., Sacks, W., Sun, Y., Tang, J., and Yang, Z.-L.: Technical Description of version 4.5 of the Community Land Model (CLM), National Center for Atmospheric Research, Boulder, CO, USA, 2013.
- Phillips, J. R., Brice, D. J., Hanson, P. J., Childs, J., Iversen, C. M., Norby, R. J., and Warren, J. M.: SPRUCE pretreatment plant tissue analyses, 2009 through 2013, https://doi.org/10.3334/CDIAC/spruce.038, 2017.
- Renaudin, M., Khlifa, R., Legault, S., Kembel, S. W., Kneeshaw, D., Moore, J.-D., and Houle, D.: Long-Term Simulated Nitrogen Deposition Has Moderate Impacts on Soil Microbial Communities across Three Bioclimatic Domains of the Eastern Canadian Forest, Forests, 14, 1124, https://doi.org/10.3390/f14061124, 2023.
- Ricciuto, D., Sargsyan, K., and Thornton, P.: The impact of parametric uncertainties on biogeochemistry in the E3SM Land Model, J. Adv. Model. Earth Syst., 10, 297–319, https://doi.org/10.1002/2017MS000962, 2018.
- Rossi, S., Bordeleau, A., Houle, D., and Morin, H.: Effect of chronic ammonium nitrate addition on the ectomycorrhizal community in a black spruce stand, Can. J. For. Res., 42, 1204–1212, https://doi.org/10.1139/x11-176, 2012.
- Salmon, V. G., Brice, D. J., Bridgham, S., Childs, J., Graham, J., Griffiths, N. A., Hofmockel, K., Iversen, C. M., Jicha, T. M., Kolka, R. K., Kostka, J. E., Malhotra, A., Norby, R. J., Phillips, J. R., Ricciuto, D., Schadt, C. W., Sebestyen, S. D., Shi, X., Walker, A. P., Warren, J. M., Weston, D. J., Yang, X., and Hanson, P. J.: Nitrogen and phosphorus cycling in an ombrotrophic peatland: a benchmark for assessing change, Plant Soil, 466, 649–674, https://doi.org/10.1007/s11104-021-05065-x, 2021.
- Sanders-DeMott, R., Sorensen, P. O., Reinmann, A. B., and Templer, P. H.: Growing season warming and winter freeze-thaw cycles reduce root nitrogen uptake capacity and increase soil solution nitrogen in a northern forest ecosystem, Biogeochemistry, 137, 337–349, https://doi.org/10.1007/s10533-018-0422-5, 2018.
- Shao, S., Wu, J., He, H., Moore, T. R., Bubier, J., Larmola, T., Juutinen, S., and Roulet, N. T.: Ericoid mycorrhizal fungi mediate the response of ombrotrophic peatlands to fertilization: a modeling study, New Phytol., 238, 80–95, https://doi.org/10.1111/nph.18555, 2023.
- Struyf, E., Kotowski, W., Jacobs, S., Van Damme, S., Bal, K., Opdekamp, W., Backx, H., Van Pelt, D., and Meire, P.: Tracing Si–N–P ecosystem-pathways: is relative uptake in riparian vegetation influenced by soil waterlogging, mowing management and species diversity?, Hydrobiologia, 674, 41–50, https://doi.org/10.1007/s10750-011-0737-x, 2011.
- Thornton, P. E. and Rosenbloom, N. A.: Ecosystem model spin-up: Estimating steady state conditions in a coupled terrestrial carbon and nitrogen cycle model, Ecological Modelling, 189, 25–48, https://doi.org/10.1016/j.ecolmodel.2005.04.008, 2005.

Van Tichelen, K. K. and Colpaert, J. V.: Kinetics of phosphate absorption by mycorrhizal and non-mycorrhizal Scots pine seedlings, Physiologia Plantarum, 110, 96–103, https://doi.org/10.1034/j.1399-3054.2000.110113.x, 2000.

Vesala, R., Kiheri, H., Hobbie, E. A., Van Dijk, N., Dise, N., and Larmola, T.: Atmospheric nitrogen enrichment changes nutrient stoichiometry and reduces fungal N supply to peatland ericoid mycorrhizal shrubs, Science of The Total Environment, 794, 148737, https://doi.org/10.1016/j.scitotenv.2021.148737, 2021.

Ward, E. B., Duguid, M. C., Kuebbing, S. E., Lendemer, J. C., and Bradford, M. A.: The functional role of ericoid mycorrhizal plants and fungi on carbon and nitrogen dynamics in forests, New Phytol., 235, 1701–1718, https://doi.org/10.1111/nph.18307, 2022.

Weber, S. E., Childs, J., Latimer, J., Hanson, P. J., Salmon, V. G., Schwaner, G., and Iversen, C. M.: Warming and elevated CO2 cause greater and deeper root growth by shrubs in a boreal bog, https://doi.org/10.1101/2025.06.26.661811, 30 June 2025.

Wu, Y. and Blodau, C.: PEATBOG: a biogeochemical model for analyzing coupled carbon and nitrogen dynamics in northern peatlands, Geosci. Model Dev., 6, 1173–1207, https://doi.org/10.5194/gmd-6-1173-2013, 2013.

Xie, L., Zhou, X., Liu, Q., Zhao, C., and Yin, C.: Inorganic nitrogen uptake rate of *Picea asperata* curtailed by fine root acclimation to water and nitrogen supply and further by ectomycorrhizae, Physiologia Plantarum, 173, 2130–2141, https://doi.org/10.1111/ppl.13562, 2021.